SIMSHOL: A Predictive Simulation Approach to Inform Helicopter-Ship Clearance Trials

Wajih A. Memon,[*] Ieuan Owen,[†] and Mark D. White[‡]
University of Liverpool, Liverpool, England L69 3GH, United Kingdom

This paper presents the development of a simulation framework, SIMSHOL, which has a predictive capability to inform and support real-world Ship Helicopter Operating Limit (SHOL) trials for a range of helicopter-ship combinations. SIMSHOL is a desktop-based predictive simulation tool that presents an objectively optimized human pilot modelling technique within an integrated pilot-vehicle-environment that represents the Helicopter Ship Dynamic Interface (HSDI). The overall scheme employs a multi-loop pursuit pilot model, a linearized helicopter flight dynamics model with a new enhanced spatial turbulence model, together with an objective optimization loop. To simulate the ship airwake turbulence effect, a new spatial airwake disturbance modelling technique has been developed which, in real-time, captures the spectral characteristics of the turbulence around the ship from a CFD-computed ship airwake. Time and frequency domain comparisons have been made between SIMSHOL and piloted simulation flight trial experiments. It was observed that the performance of the SIMSHOL tool in maintaining sufficient clearance between the aircraft and the ship's landing deck and hangar, whilst rejecting airwake disturbances, is well within the desired task performance boundaries. These investigations have shown that the tool is capable of representing the dynamics of a pilot-vehicle-task system in the challenging HSDI environment. Moreover, an automatic error-minimization based response optimization methodology has been developed and utilized which uses the iterative Gradient Descent optimization algorithm to objectively tune the pilot-vehicle loop transfer functions to represent a pilot's performance in the simulator. The results show that SIMSHOL is able to predict operational limits for a range of different helicopter-ship and environmental combinations.

Nomenclature

$\boldsymbol{A}$, $\boldsymbol{B}$, $\boldsymbol{C}$	=	Linearized flight dynamics model system, input and output matrices.
k_p, k_ϕ, k_v, k_y	=	Pilot model lateral channel loop gains.
k_q, k_θ, k_u, k_x	=	Pilot model longitudinal channel loop gains.
k_i, k_r, k_ψ	=	Pilot model pedal channel loop gains.

[*]Ph.D. Candidate, School of Engineering, The University of Liverpool.
[†]Emeritus Professor of Mechanical Engineering, School of Engineering, The University of Liverpool.
[‡]Senior Lecturer, School of Engineering, The University of Liverpool.

$k_{\dot{w}}$, k_w, k_h	=	Pilot model collective channel loop gains.
k_r, k_{ro}, k_p, k_{po}	=	Pilot model sequential loop gains, innermost to outermost loop.
$\dot{P}$, $\dot{Q}$, $\dot{R}$	=	Helicopter angular accelerations (rad/s^2).
P, Q, R	=	Helicopter angular velocities (rad/s).
R_m, R_t	=	Helicopter main and tail rotor radii (ft).
U, V, W	=	Helicopter fuselage linear velocities (ft/s).
$\dot{U}$, $\dot{V}$, $\dot{W}$	=	Helicopter fuselage linear accelerations (ft/s^2).
U_∞	=	Freestream wind velocity (ft/s).
u_a, v_a, w_a	=	Airwake velocity components (ft/s).
u'_a, v'_a, w'_a	=	Airwake velocity fluctuations (ft/s).
U_L	=	Mean wind speed at the deck landing spot (ft/s).
$\boldsymbol{x}$, $\boldsymbol{y}$, $\boldsymbol{u}$	=	Linearized flight dynamics model state, output and input vectors.
X, Y, Z	=	Helicopter fuselage linear displacements (ft).
x_a, y_a, z_a	=	Airwake structured domain node location coordinates (ft).
$X_{c.g}$, $Y_{c.g}$, $Z_{c.g}$	=	Ship's linear displacement at its c.g. (ft).
X_d, Y_d, Z_d	=	Ship's linear displacement at deck landing spot (ft).
X_{l2o}, Y_{l2o}, Z_{l2o}	=	Positions from the ship's c.g. to the landing spot (ft).
σ_T	=	Total RMS turbulence intensity (ft/s).
σ_u, σ_v, σ_w	=	Airwake RMS turbulence intensities (ft/s).
δ_{Long}, δ_{Lat}, δ_{Coll}, δ_{Ped}	=	Pilot control deflections (%).
δ_{Long_C}, δ_{Lat_C}, δ_{Coll_C}, δ_{Ped_C}	=	Actual pilot model control deflections (%).
δ_{Long_T}, δ_{Lat_T}, δ_{Coll_T}, δ_{Ped_T}	=	Enhanced spatial CETI model control deflections (%).
ϕ, θ, ψ	=	Helicopter fuselage attitudes (rad).
ϕ_s, θ_s, ψ_s	=	Ship's attitudes (deg).
w_n	=	White noise.

Subscripts

a	=	Airwake domain axis.
C	=	Actual control input.
C+T	=	Total control input.
d	=	Ship's landing deck.
l2o	=	Ship's landing spot to its c.g. location.
s	=	Ship axis.
T	=	CETI turbulence input.

I. Introduction

The launch and recovery of helicopters from and to naval ships are carried out in challenging conditions, which are unique to the maritime environment. The combination of a confined ship landing deck, irregular ship motion, sea spray and unsteady airflow over and around the ship's landing deck and superstructure, produce a high risk to, and operational demand on, the helicopter, ship, and crew. Together, these elements form the Helicopter Ship Dynamic Interface (HSDI) environment [1] (Fig. 1).

Fig. 1 HSDI environment

To determine the limitations of the safe operation of helicopters to and from ships, a safety envelope known as the Ship Helicopter Operating Limit (SHOL) is constructed, normally through First of Class Flight Trials (FOCFTs), for every in-service combination of helicopter and ship. The SHOL defines the safe environmental conditions for the helicopter launch and recovery operations, which subsequently provides operational guidelines to the pilot and crew [2]. The larger the SHOL envelope, the greater the operational capability of a given helicopter landing on a given ship. FOCFTs are performed at sea and are inevitably expensive and it can typically take weeks to construct a full SHOL envelope. Often the full range of wind and sea conditions may not be available during the trials, resulting in the construction of a more conservative SHOL [3]. An example of a SHOL envelope is shown in Fig. 2.

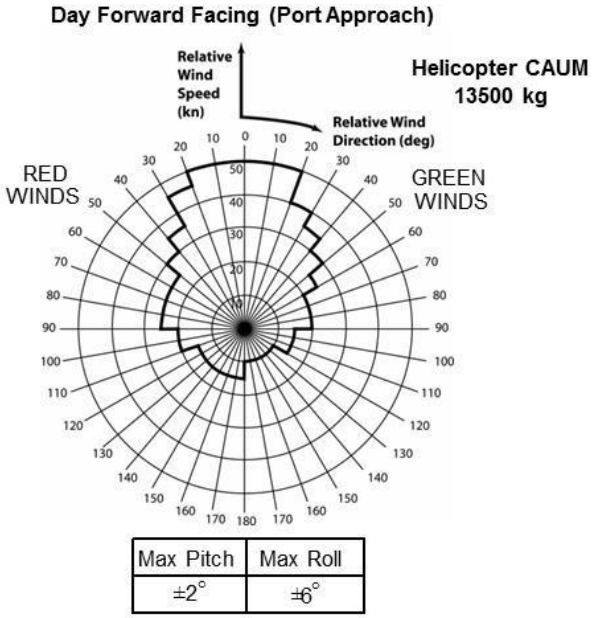

Fig. 2 Typical SHOL diagram [4]

The SHOL consists of radial and circumferential lines of wind azimuth and magnitude, respectively, representing the Wind Over Deck (WOD) condition measured at the ship's anemometer. The SHOL limit is shown as a bold black line, and the area inside this boundary indicates the combinations of wind speed/direction for which it is safe to land the helicopter.

Because of the challenging environmental conditions described above, Modelling and Simulation (M&S) of the HSDI environment is being developed and deployed in flight simulators to investigate these operational and meteorological risks, with the intention of making SHOL testing safer, quicker, and more cost-effective [5-8]. Whilst not trying to fully replace at-sea testing, M&S aims to inform the key test points or "Hot Spots" to test at sea.

Over the past few years, flight simulators have been utilized to better understand the complex interaction between the helicopter and ship within the challenging HSDI environment, and for deriving helicopter/ship operational guidelines and constructing preliminary simulated SHOL envelopes [6-14]. The aim has been to offer a wide range of benefits to the at-sea SHOL development process by testing various HSDI scenarios and environmental conditions repeatedly with a range of pilots, prior to the FOCFTs. A notable milestone in the use of M&S in maritime aircraft clearance trials was the use of piloted flight simulation in preparation for the F-35B Lightning II FOCFTs on the UK's new aircraft carrier, HMS Queen Elizabeth [15]. To emulate this success, it would be desirable to have M&S tools that can inform helicopter-ship FOCFTs; the development of such a toolset is the theme of this paper.

The Flight Science and Technology research group at the University of Liverpool operates a fully reconfigurable full-motion research simulator, HELIFLIGHT-R (Fig. 3) [16], for the purpose of analyzing flight handling qualities, pilot workload assessment, flight model development and simulation fidelity criteria. It has been at the forefront of research to develop high-fidelity HSDI simulation environments [3,10-15].

HELIFLIGHT-R has been successfully used in several previous HSDI simulation research projects, such as shipboard operations for simulated SHOL prediction work on a Type-23 Frigate, a Wave Class Auxiliary Oiler [3], and the Queen Elizabeth Class (QEC) aircraft carrier [13,15]. The helicopter flight dynamics model used in these studies, and in the present study, was a generic FLIGHTLAB helicopter model [17] representing a SH-60B Seahawk helicopter [18].

Fig. 3 HELIFLIGHT-R simulator (foreground)

Whilst the authors continue to be engaged in research to further develop full-motion flight simulators and its fidelity requirements to inform SHOL trials [19-21], in this paper, a complementary modelling approach is presented in which an offline desktop-based predictive simulation tool has been developed to assess the overall HSDI pilot-vehicle-task-environment system to determine an initial SHOL. The developed tool has the capability of representing the dynamics of the combined pilot-vehicle system in the particularly demanding HSDI environment, which includes the effects of a CFD-computed ship's airwake and representative deck motion. The tool, SIMSHOL, has been used in conjunction with Piloted Simulation Flight Trials (PSFTs) conducted in HELIFLIGHT-R to develop an automatic response optimization methodology that objectively tunes the pilot-vehicle loop transfer functions, using a machine learning based optimization algorithm to design an optimized HSDI simulation framework. To accurately simulate the ship airwake turbulence effect within the SIMSHOL tool's offline simulations, a new enhanced spatial airwake disturbance modelling technique has been developed. This improves the generic stochastic turbulence model, which, in real-time, captures the spectral characteristics of the turbulence around the ship from CFD-computed ship airwakes. The proposed tool offers the potential of a faster, cheaper, and more efficient method for operational analysis of launch and recovery tasks for different combinations of helicopters and ships, and for the aerodynamic assessment of the ship superstructure design. The aim is to predict and examine mission effectiveness, pilot cueing, environmental effects, and task performance for existing as well as new helicopter-ship combinations prior to the PSFTs and the real-world FOCFTs. The tool is not offered as a substitute for the piloted trials, rather it will complement such operations.

Figure 4 shows the structure of the predictive simulation tool, SIMSHOL, which includes a multi-loop multi-axis pursuit pilot model loop combined with approximated human sensory cue feedback, linearized helicopter dynamics, a new equivalent enhanced spatial CFD-based ship airwake turbulence model, and ship motion which, combined, represent the integrated HSDI simulation environment.

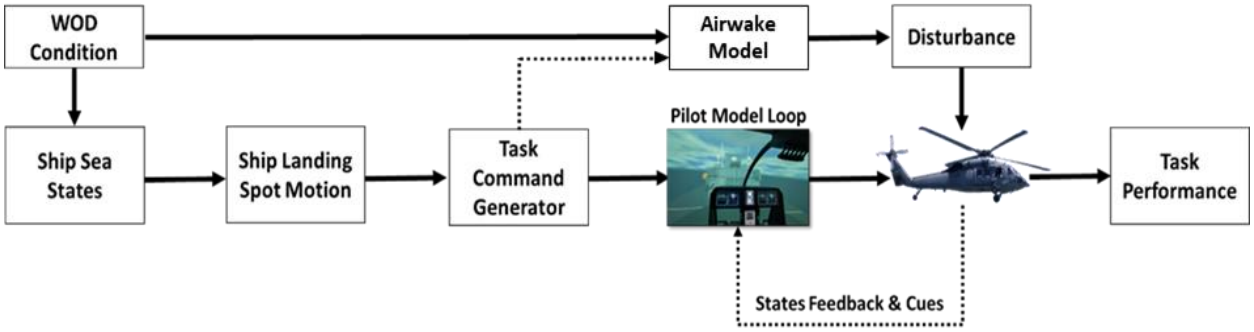

Fig. 4 Top level SIMSHOL tool structure

In developing SIMSHOL, two multi-loop flight tasks have been simulated and examined. The ADS-33E-PRF Precision Hover task [22] was examined first, being analogous to a hover flight condition in the helicopter-ship recovery task. This task was used for the initial analysis and pre-validation of the tool and for the pre-development of the response optimization methodology. Second, an HSDI deck landing task [2] was constructed and examined in which the mission of interest was the successful recovery of a simulated helicopter, configured to represent a SH-60B Seahawk, to the deck of a single-spot destroyer, utilizing a newly developed spatial turbulence integration technique. The simulations of both the tasks were compared with previous PSFTs and optimized using a newly proposed automatic response optimization technique. Finally, in conjunction with the PSFTs, the devised response optimization methodology was used to design a universal setting of the SIMSHOL tool for the optimized HSDI deck landings on five different naval ships (QEC, Wave Class Oiler, single-spot destroyer similar to the UK's Type 45, Simple Frigate Shape v2 and a UK Type 23 Frigate) at a particular WOD condition.

The paper is organized as follows: Section II discusses existing approaches to helicopter-ship desktop simulation tools based on different pilot modelling techniques, whilst Section III defines the helicopter flight dynamics models used for the two flight conditions considered and their comparisons with the non-linear FLIGHTLAB model. Section IV explains the pilot model loop design procedure whilst Section V shows a land-based task and the model optimization approach using the developed SIMSHOL tool. Section VI describes the HSDI task design in SIMSHOL, including the augmented spatial airwake turbulence technique and presents simulation results. Section VII details the response optimization methodology developed for the model's transfer function objective optimization and for designing a universal SIMSHOL configuration. Conclusions and future work are presented in Section VIII.

II. Background of HSDI M&S Predictive Tools

A number of desktop helicopter-ship simulation tools have previously been developed based on a range of pilot modelling techniques. Lee, et al. developed a simulation of a UH-60A GENHEL simulated helicopter operating from a Landing Helicopter Assault class ship using a compensatory optimal control pilot model [23]. Moon, et al. investigated the operation of a BO-105 simulated helicopter operating from a TMV 114 fast ferry using a compensatory optimal control pilot model [24], whilst Jarrett and Manso studied the effect of a ship's airwake on an MRH-90 helicopter model recovering to a Landing Helicopter Dock class ship using a Proportional Integral Derivative controller based virtual pilot model [25]. Figueira, et al. developed a modified SYCOS classical pilot model and analyzed deck landings on a generic Light Stealth Frigate using the *PycsHel* Simulation facility [26].

However, these techniques only partially represent the overall human central nervous system, due to the absence of some human sensory modelling elements, particularly the visual, vestibular, and proprioceptive systems which provide motion perception characteristics to the pilot model. The inclusion of these elements increases the fidelity of the pilot model by approximating the dynamics of the human sensory systems, which are important for tasks where the pilot uses information/cues from different perceptual modalities, i.e., vestibular motion, and visual cues, to successfully accomplish the task [27]. Recent work by the authors on establishing simulator visual-vestibular motion fidelity requirements for simulated shipboard operations have demonstrated the importance and sensitivity of different perceptual modalities in piloted simulations. It was found that the pilot captures cues on the aircraft states from vestibular and visual motion cues when conducting a task which is highly dependent upon the task requirements and fidelity of the motion perceptual modalities [21].

Hess [28] introduced a simplified technique of using a compensatory structural pilot model for modelling helicopter operations near ships which includes all the human sensory feedback systems: vestibular, proprioceptive, visual, and neuromuscular dynamics. However, whilst the pilot model is capable of representing a compensatory control strategy, in reality, the helicopter shipboard task is a pursuit tracking task where the target (i.e., the ship's landing deck) is continuously and independently moving [1], imposing additional requirements to the piloted task.

In a compensatory tracking task, feedback consisting of an indicator and a fixed reference point (i.e., the target) is provided to the pilot, and the task is to maintain the indicator on the reference point by compensating for the movements of the indicator via control inputs. An ideal compensatory tracking task would be the one in which there will be no further movement once the target location is achieved. A pursuit tracking task, on the other hand, is one in which the target moves due to external outside influences and the operator controls the follower in such a way as to keep it superimposed over the target. An ideal pursuit tracking would result in continuous movement (e.g., Superslide task [29], and HSDI task [2]). In a pursuit task, the external visual reference and sensory feedback systems are references naturally utilized by the pilot to perceive more information from the environment to be able to successfully and safely accomplish the task [30,31].

Therefore, in this study, the pilot modelling approach used in the development of the SIMSHOL tool is based on a pursuit pilot tracking technique, incorporating the necessary human motion perception features (e.g., visual, vestibular, and proprioceptive system) and is capable of representing multi-loop tasks. These features make the developed SHOL predictive tool (i.e., SIMSHOL) more applicable for the HSDI deck landing task simulations than has previously been achieved due to the task-specific characteristics, detailed in Section IV.

III. Helicopter Flight Dynamics

Among the different elements of SIMSHOL's structure shown in Fig. 4, one of the critical components of the pilot model loop design is a representative linearized helicopter flight dynamics model, which should accurately capture the dynamics of the non-linear full-scale model; this was the first step in the SIMSHOL design. The linearized model was used to simplify the overall construction and design of the SIMSHOL tool. The flight dynamics model used was a FLIGHTLAB [17] model representative of an SH-60B Seahawk helicopter, Fig. 5. The model has been used in several instances for simulated HSDI PSFTs in the HELIFLIGHT-R simulator [3,10-16,19-21], as detailed in Section I.

Fig. 5 SH-60B helicopter

A multi-axis 6 Degree of Freedom (DoF), 9-state state-space linearized model (Eqn. 1) of an SH-60B helicopter was extracted from a non-linear FLIGHTLAB model.

$$(\boldsymbol{x}, \dot{\boldsymbol{x}}, \boldsymbol{u}) = 0, \quad \boldsymbol{x} \in R^9, \boldsymbol{u} \in R^4 \tag{1}$$

Two flight conditions are examined in this paper. The first was a hover flight trim condition, chosen for initial pilot model loop gains selection test and preliminary task analysis by simulating the ADS-33E-PRF Precision Hover task [22]. The second was a 25 kts low-speed forward flight condition to simulate the HSDI shipboard landing task [2]. The resulting Linear Time Invariant (LTI) system is described by Eqn. 2:

$$\dot{\boldsymbol{x}} = \boldsymbol{A}.\,\boldsymbol{x} + \boldsymbol{B}.\,\boldsymbol{u} \quad \boldsymbol{y} = \boldsymbol{C}.\,\boldsymbol{x} \tag{2}$$

$$\boldsymbol{x} = [\phi, \theta, \psi, U, V, W, P, Q, R]$$

$$\boldsymbol{u} = [\delta_{Long}, \delta_{Lat}, \delta_{Coll}, \delta_{Ped}]$$

where $\boldsymbol{x}$, $\boldsymbol{y}$ and $\boldsymbol{u}$ are the state, output and input vectors, respectively, and $\boldsymbol{A}$, $\boldsymbol{B}$ and $\boldsymbol{C}$ are the system, input and output matrices, respectively; (ϕ, θ, ψ) are the helicopter fuselage attitudes; (*U, V, W*) are the helicopter fuselage linear velocities; (*P, Q, R*) are the helicopter fuselage angular rates; and (δ_{Long}, δ_{Lat}, δ_{Coll}, δ_{Ped}) are the pilot control inceptor deflections.

Figures 6 to 9 shows the comparison of the linear and non-linear SH-60B FLIGHTLAB vehicle model responses to a longitudinal and lateral 3-2-1-1 control input to hover and low-speed flight dynamic models, detailed in the following Sections III.A and III.B, respectively.

A. Hover Condition Flight Model

The linearized vehicle model LTI system matrices for the hover flight condition are given in the Appendix. Figures 6 and 7 show the on- and off-axis comparisons of the linear and non-linear flight model responses to longitudinal and lateral stick control inputs. Overall, the observed responses of the linearized models show good agreement with the non-linear model.

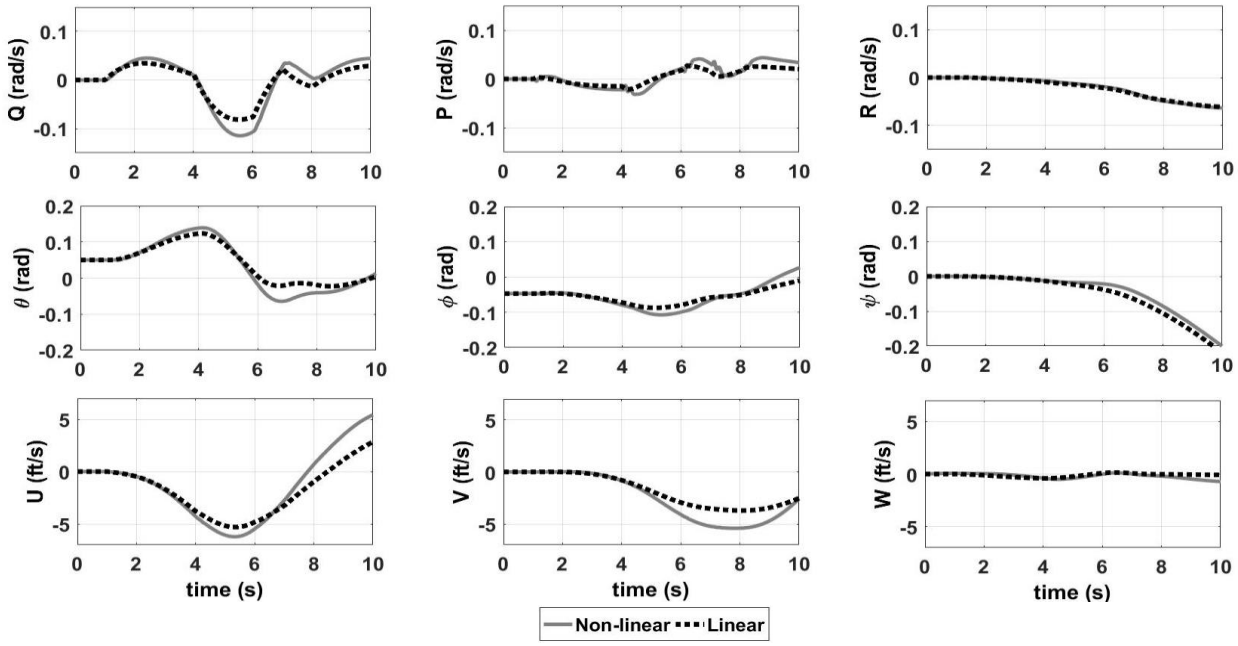

Fig. 6 Longitudinal input responses in hover dynamics

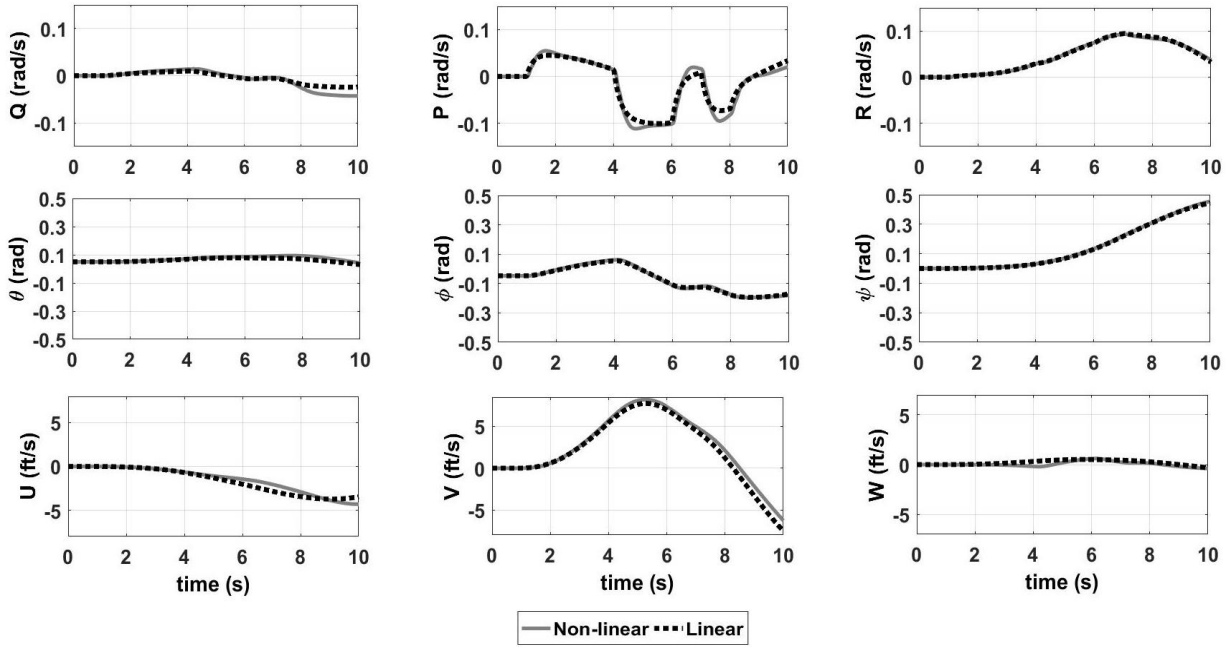

Fig. 7 Lateral input responses in hover dynamics

B. Low-Speed Forward Condition Flight Model

The linearized vehicle model LTI system matrices for the low-speed flight condition (trimmed at 25 kts indicated airspeed comprised of 12 kts ground speed and 13 kts relative headwind) are given in the Appendix. Figures 8 and 9 show the on- and off-axis comparisons of the linear and non-linear flight model responses to longitudinal and lateral stick control inputs.

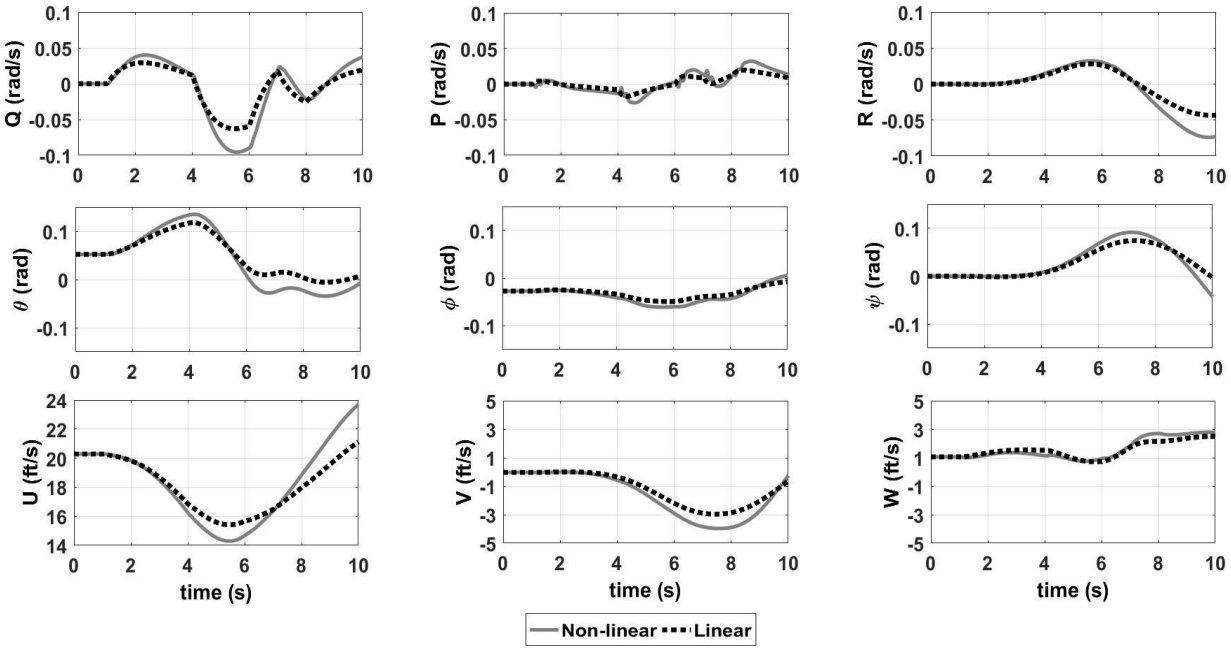

Fig. 8 Longitudinal input responses in low-speed forward flight dynamics

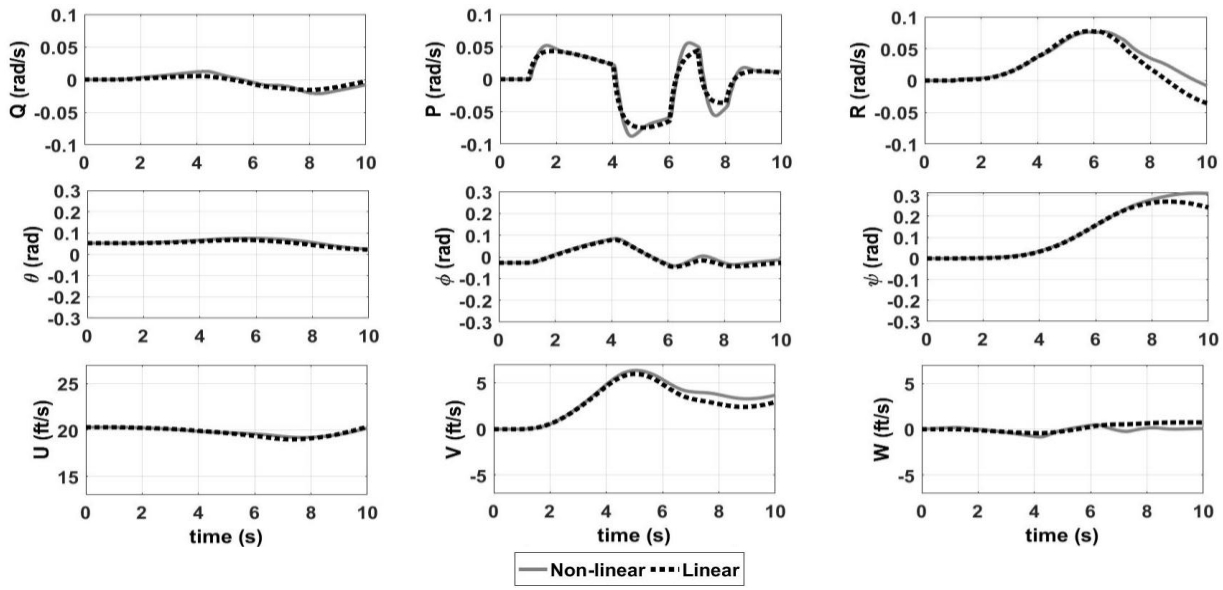

Fig. 9 Lateral input responses in low-speed forward flight dynamics

The linearized model captures the overall behaviour of the non-linear helicopter dynamics well, which is sufficient for the pilot loop design within SIMSHOL. The missing dynamics in the linearized model, such as lead-lag dampers, flapping, and inflow, possibly account for the small discrepancies in some off-axis responses. In practice, the sampling time required for the determination of the pilot loop gains to design the pilot feedback loop of the SIMSHOL tool is shorter than the response time shown here (approximately up to 4 secs), as will be seen in the pilot model loop design in Section IV, Fig. 15. Therefore, the agreement between the nonlinear and linearized models for such a short time interval was considered suitable for this application.

IV. Pilot Model Loop Design

The pilot modelling technique used in the development of the SIMSHOL tool was first introduced by Hess [32] and has now been applied, examined, and augmented in an HSDI environment in this paper. The technique is based on a pursuit pilot tracking model [32] capable of representing multi-loop tasks (two or more control inputs simultaneously) and incorporates all the human motion sensory equalization features (e.g., visual, vestibular, and proprioceptive system feedback) in a vehicular control manner [33]. These features make the model more applicable for the HSDI deck landing task simulations as it is a complex pursuit tracking task where the pilot derives aircraft state information/feedback from various sources such as the visual scene, relative aircraft motion, muscle motor movements, and instruments, together with external influencing factors such as airwake disturbances and landing deck motion [1]. In this paper, a new spatial airwake integration technique has been developed, augmenting the generic CETI turbulence model to better represent a time-accurate CFD ship airwake in the SIMSHOL simulations, detailed in Section VI.C. A response optimization methodology has also been developed in conjunction with the PSFTs and

integrated with the SIMSHOL tool to objectively tune the system to produce optimized responses representing pilot behaviour in a flight simulator, detailed in Section VII. Figure 10 shows the detailed SIMSHOL structure with the proposed Optimization and HSDI simulation environment (i.e., Ship motion and CFD ship airwake) development loops.

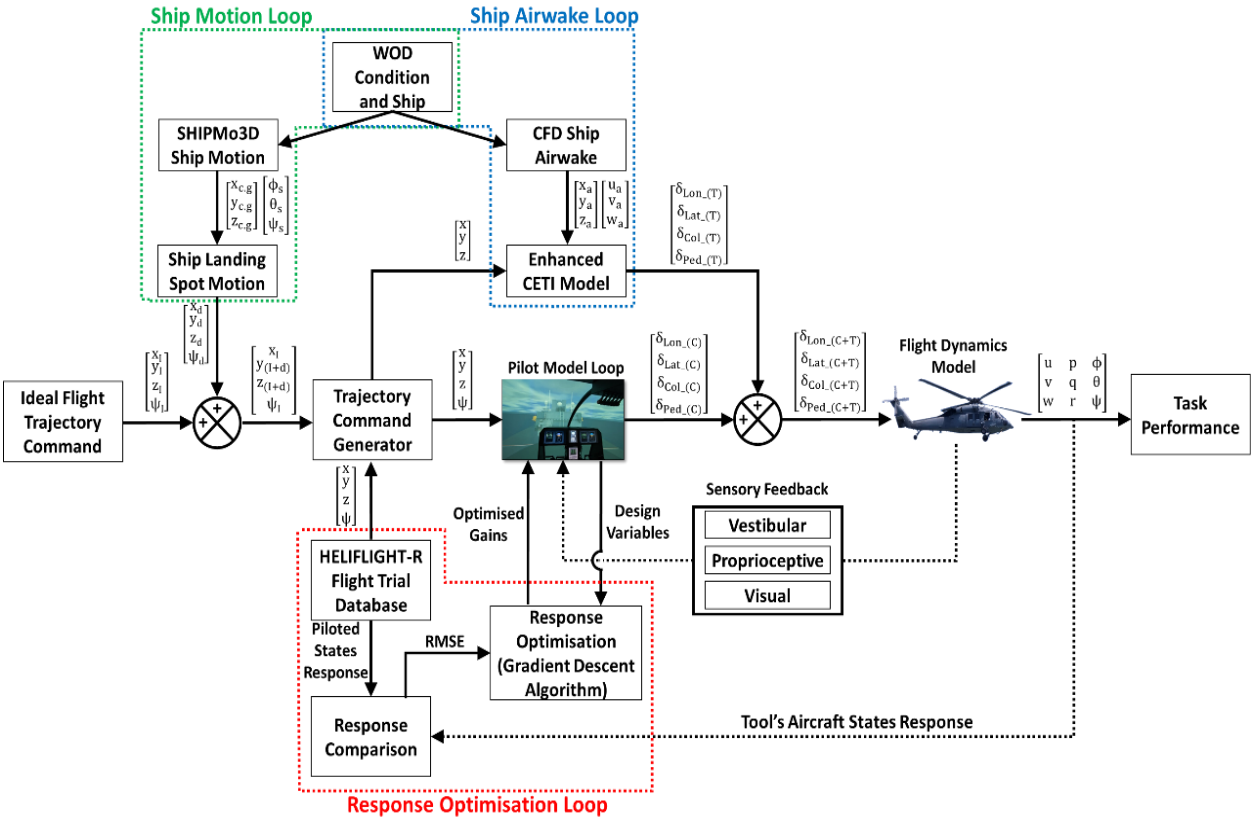

Fig. 10 Detailed SIMSHOL structure

The pilot model loop consists of three main systems: Command Generator, Pilot Loop, and Vehicle Dynamics, as shown earlier in Fig. 4. The command generator provides a flight trajectory input that is to be followed by the pilot model, consisting of an array of four inputs, *X, Y, Z, ψ* (one for each channel). The pilot loop consists of the feedback loops that require the determination of pilot gains using frequency domain (F-D) and/or time domain (T-D) techniques. Vehicle dynamics consist of a linearized state-space model of an SH-60B Helicopter extracted from FLIGHTLAB for a particular flight condition, as described in Section III. Figure 11 shows the feedback "information" sequential loops of the pilot model, innermost to outermost. Within each loop, the gain ($k_r \rightarrow k_p \rightarrow k_{ro} \rightarrow k_{po}$) is selected based on the requirement that the model should be capable of performing the specified task and should produce representative responses. To meet these rules, the gains are selected based on F-D and T-D criteria detailed later in this section.

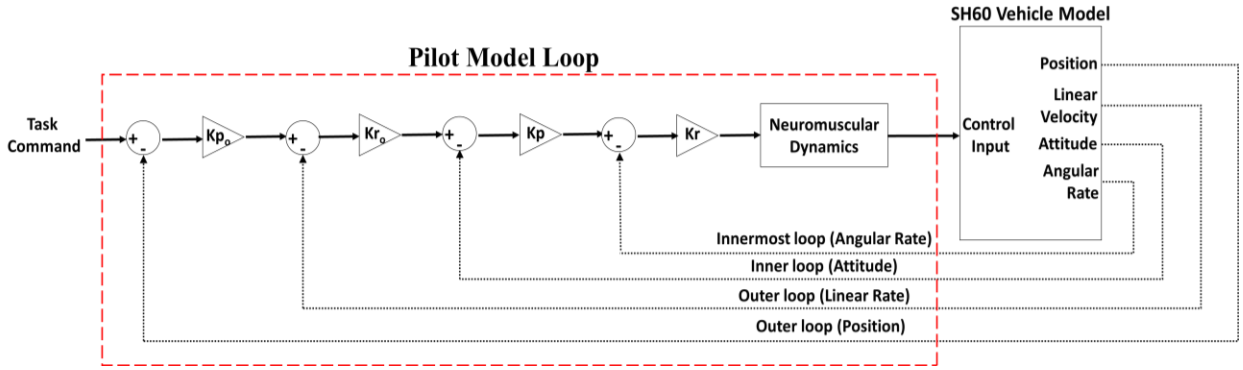

Fig. 11 Sequential pilot model loops

Motion cues in flight simulators are perceived from visual information projected onto the human eye (i.e., Vection), from a simulator's movement detected by the vestibular system present in the human ear (i.e., vestibular cues) and somatosensory receptors consisting of tactile and proprioceptive senses used to sense the change of forces on the human body and relative body parts position [34]. The vestibular system consists of two parts: the Semi-Circular Canals (SCC) and the Otoliths (Oto). The SCC acts as a damped angular accelerometer which senses the angular rates, and Oto senses the linear accelerations.

Figures 12 and 13 show the SIMULINK pilot model loop structure arrangement for the longitudinal and lateral channels, respectively. The combination of the vestibular (SSC and/or Oto) and proprioceptive system provides the aircraft's rate response motion feedback as a weighted sum of the combined cueing system, see Figs. 12 and 13. The proprioceptive feedback is weighted at 75 % and the vestibular at 25 %, as discussed in [35]. The main difference between the proprioceptive system and the vestibular system is the way in which they capture the motion information from the stimuli. The proprioceptive system captures information from the body joints and muscle receptors as a result of the movement; therefore, a suitable order transfer function of the aircraft's rate response output to corresponding control input is extracted from the vehicle models under examination, to approximate the rate response feedback via the proprioceptive system. Table 1 shows the proprioceptive transfer functions derived in this study for each channel of the linearized models described in Section III. The vestibular system, on the other hand, captures the information of the physical movement that the body is subjected to, directly using 'Oto' and 'SSC' vestibular organs present in the human ear [35]; therefore, direct weighted feedback is input to the loop. Since physical movement is needed for activation of receptors of both the proprioceptive and vestibular systems, the two are often not separated and process motion perception in combination [36].

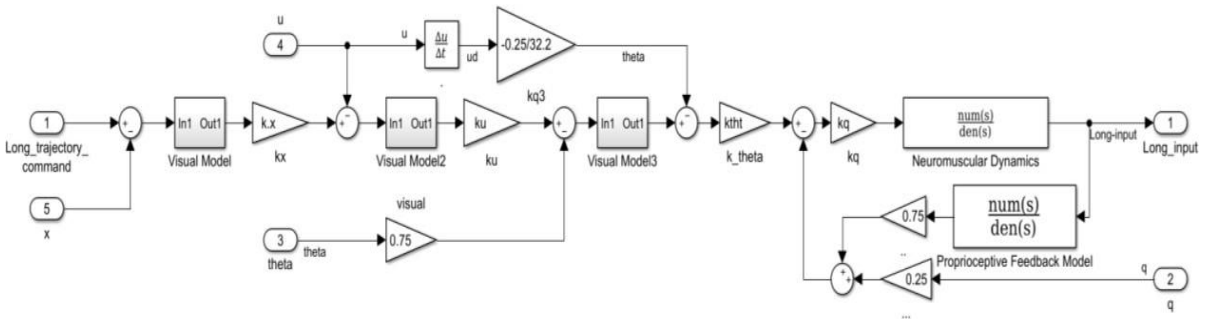

Fig. 12 Longitudinal pilot model loop

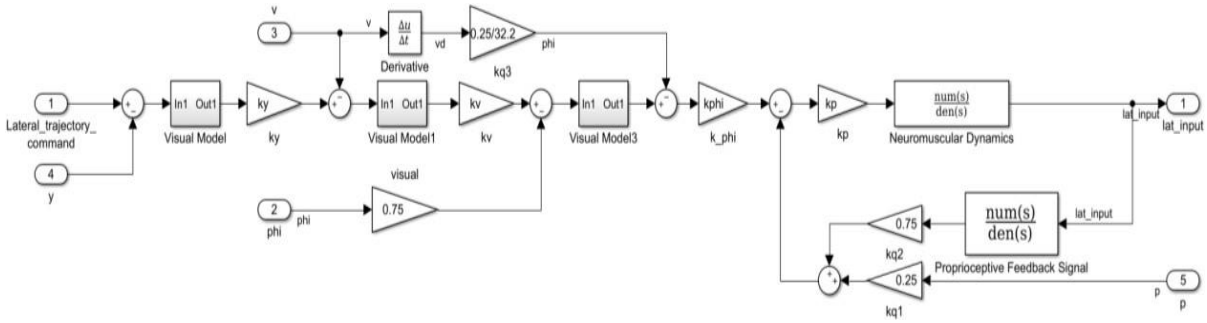

Fig. 13 Lateral pilot model loop

The combination of the visual-vestibular system provides motion feedback of the aircraft's attitude response, see Figs. 12 and 13. The visual system provides the aircraft attitude cues feedback via external visual reference to the objects in the outside world, while the Otoliths of the vestibular system provides additional surrogate pitch and roll attitude cues feedback via the perception of the linear surge and sway accelerations cues, respectively. Combination of the visual-vestibular system is also employed in a weighted fashion, similar to the vestibular-proprioceptive combination; the visual feedback is weighted at 75 %, and the vestibular at 25 %, as discussed in [35,38]. Altogether, the visual-vestibular-proprioceptive sensory feedback system produces a good approximate representation of overall self-motion perception of the human pilot [33,36].

For the design of the pilot model loop, F-D and T-D criteria described in [32] and [39], respectively, were initially employed in the selection of the appropriate pilot gains to build the SIMSHOL simulation scenarios and analyze the task simulations. Later, these gains served as a baseline setting for the development and application of the response optimization methodology to help tune the system objectively for optimal SIMSHOL performance, representing the pilot's behavior in the simulator. The gains selection process involves sequentially closing the loops of the pilot model by fulfilling the design requirements within each channel (longitudinal, lateral, collective, and pedal) separately, and then combining all the channels to form a 6 DoF pilot model structure. Altogether there are fourteen pilot gains to be designed, four in each of the lateral and longitudinal channels and three in each of the collective and pedal channels, see Table 2.

Table 1 Proprioceptive feedback models

Channels	Hover Flight Dynamics	Low-speed forward flight dynamics
$\frac{Q}{\delta_{Long}}$	$\frac{0.032s^4 - 0.0025s^3 + 0.0056s^2 - 0.000903s + 0.00017}{s^5 + 0.9914\,s^4 + 0.8138\,s^3 + 0.2887\,s^2 + 0.1057s + 0.03193}$	$\frac{0.03s^3 + 0.00344s^2 - 0.000281s + 8.606e-06}{s^4 + 1.568s^3 + 0.68s^2 + 0.30428s + 0.002374}$
$\frac{P}{\delta_{Lat}}$	$\frac{0.1156\,s^4 + 0.0266\,s^3 + 0.0142\,s^2 - 0.00174\,s - 3.197e-05}{s^5 + 4.84s^4 + 1.462s^3 + 1.439\,s^2 + 0.2126s + 0.1369}$	$\frac{0.07269s^3 - 0.002734s^2 + 0.0057s - 0.0005279}{s^4 + 2.306s^3 + 1.355s^2 + 0.341s + 0.0456}$
$\frac{\dot{W}}{\delta_{Coll}}$	$\frac{-0.548\,s^4 + 0.0482\,s^3 - 0.088\,s^2 - 0.0023\,s + 3.985e-06}{s^5 + 10.16s^4 + 1.781s^3 + 1.447s^2 + 0.45s + 0.0105}$	$\frac{0.0254s^4 - 0.00232s^3 + 0.00364s^2 - 9.563e-06s}{s^4 + 0.456s^3 + 0.746s^2 + 0.0664s + 0.00549}$
$\frac{\dot{R}}{\delta_{Ped}}$	$\frac{0.196\,s^4 + 0.0595\,s^3 + 0.0240\,s^2 + 0.0149s - 2.341e-06}{s^5 + 10.49\,s^5 + 5.058\,s^3 + 1.841s^2 + 0.916s + 0.128}$	$\frac{0.2145s^4 + 0.0715s^3 + 0.0281s^2 + 0.000784s}{s^4 + 0.6906s^3 + 0.387s^2 + 0.0365s + 0.0023}$

Table 2 Pilot model loop sequence

Channel	Loop Closure Sequence	Channel	Loop Closure Sequence
Longitudinal	$Q \rightarrow \theta \rightarrow U \rightarrow X$	**Collective**	$\dot{W} \rightarrow W \rightarrow Z$
Lateral	$P \rightarrow \phi \rightarrow V \rightarrow Y$	**Pedal**	$\dot{R} \rightarrow R \rightarrow \psi$

The successful selection of the pilot loop gains using the F-D technique is based on the fulfilment of the following frequency response requirements in each of the pilot loop transfer functions shown in Fig. 11. Starting from the innermost loop, the gain 'k_r' is selected such that the difference between the peak response magnitude and the mid-frequency magnitude is approximately 10 dB [32]. The gains 'k_p' and 'k_{ro}' are selected such that the open-loop crossover frequency of the inner and outer loop transfer functions is approximately 2 rad/s, and finally the gain 'k_{po}' in the outermost loop is chosen to obtain the crossover frequency of 0.667 rad/s (one-third of crossover frequency in inner loop) [32]. The Bode plots in Fig. 14 show the frequency responses obtained from the lateral channel design process, starting from the inner-most (angular rate) closed-loop pilot gain 'k_p', then the inner (attitude) open-loop pilot gain 'k_ϕ', then the outer (linear rate) loop having pilot gain 'k_v' and finally the outermost (translation) loop having pilot gain 'k_y'. The gains are adjusted/tuned until the desired criteria are achieved. The stability of the system is intact since the innermost loop remains closed throughout. This procedure is repeated for all the channels.

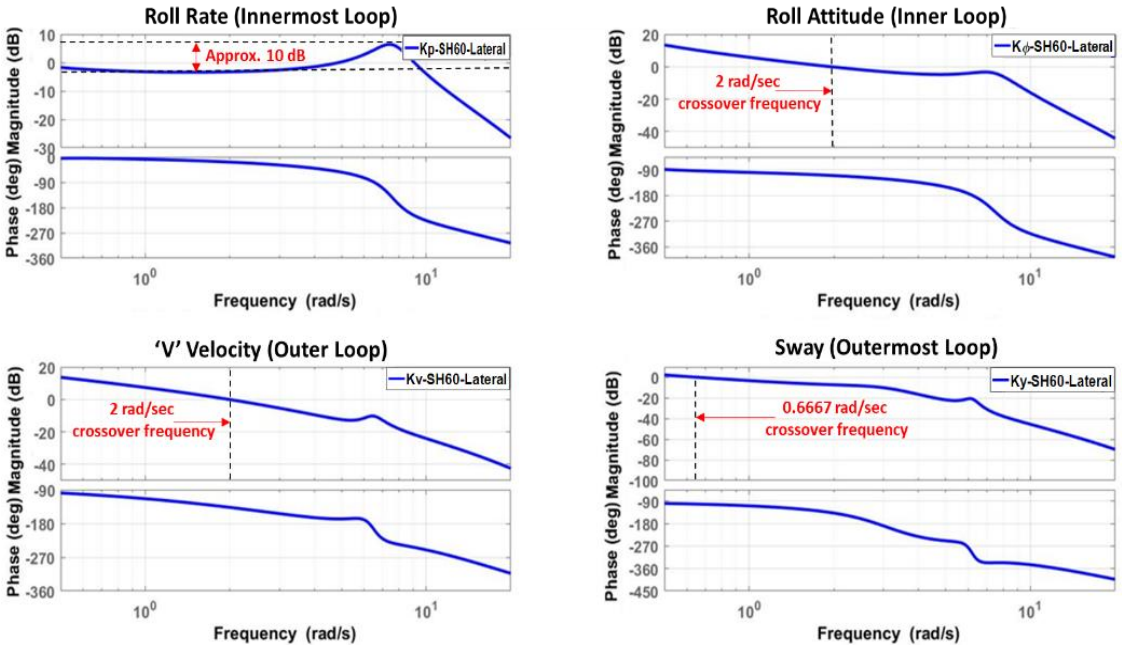

Fig. 14 F-D Technique lateral channel pilot loop design

The determination of the pilot loop gains can be performed using a T-D technique as well, consisting of an evaluation of the step and sinusoidal responses of the feedback loop transfer functions to the inputs. Figure 15 shows the T-D technique responses obtained from the lateral channel design. The sequence of the design process is the same as followed in the F-D technique, using sequential nested loop closure beginning with the innermost loop. A step input of unit amplitude is applied to the innermost loop and the gain 'k_r' is selected at which the ratio of the first overshoot to first undershoot of the response is approximately 2.25 [39], see Fig. 15. The gain value obtained can be verified with the Bode plot response obtained using the F-D technique. Once the innermost loop is closed, the inner loop gain 'k_p' is selected by exciting the open loop with a sinusoidal input of unit amplitude and frequency. The selected gain is the one for which the response amplitude and frequency are approximately the same as the input signal, see Fig. 15. This process is continued for the remaining outer linear velocity and outermost linear translation loop gains, 'k_{ro}' and 'k_{po}', respectively, as detailed in [39].

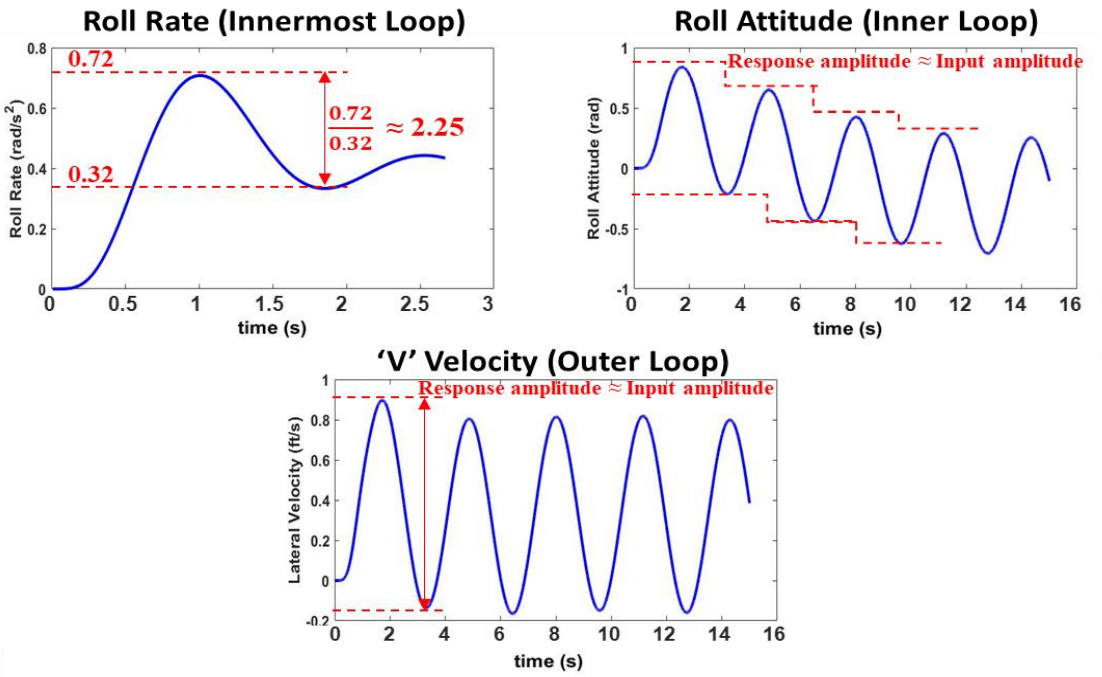

Fig. 15 T-D technique lateral channel pilot loop design

The procedure was followed to determine the initial pilot gains for both conditions, hover and low-speed forward flight, which were then objectively tuned to optimize SIMSHOL's performance by utilizing PSFTs, detailed in Section VII.

V. Precision Hover Task Simulation

Following the successful design/selection of the pilot loop gains, an initial examination of SIMSHOL was carried out by performing task simulations to compare the responses of the tool with PSFT results for a simple land-based ADS-33E-PRF Precision Hover task [22]. This was useful to aid in the pre-validation of the tool to ensure task simulation capability, initial analysis of the flight task, and objective tuning of the pilot loop gains for the response optimization. The piloted simulation data was acquired from a database of HELIFLIGHT-R piloted simulation flight trials built up over several years of in-house testing.

To perform the simulations with the tool, the model was devised with a command generator to represent a helicopter pilot performing the precision hover task using the SH-60B hover flight dynamics model referred to in Section III.A. The task course is shown in Fig. 16 and an ideal flight trajectory command input to the tool is shown in Fig. 17. The rationale for using this task for the initial model examination was:

i. the availability of sufficient piloted simulation flight trial data, and
ii. because the precision hover is a multi-axis closed-loop tracking task in which the lateral and longitudinal axes are both excited and it is useful for translation and position stability performance assessment.

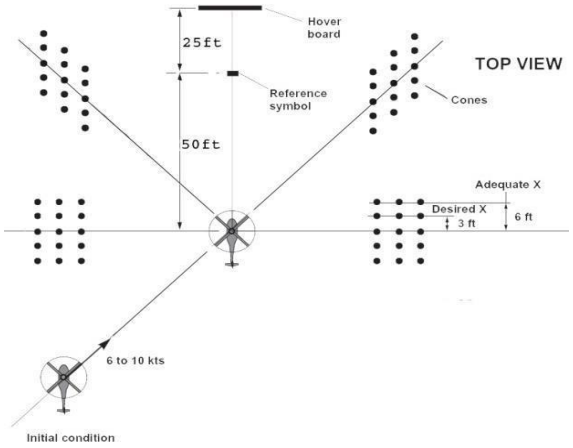

Fig. 16 ADS-33 Precision Hover task course [22]

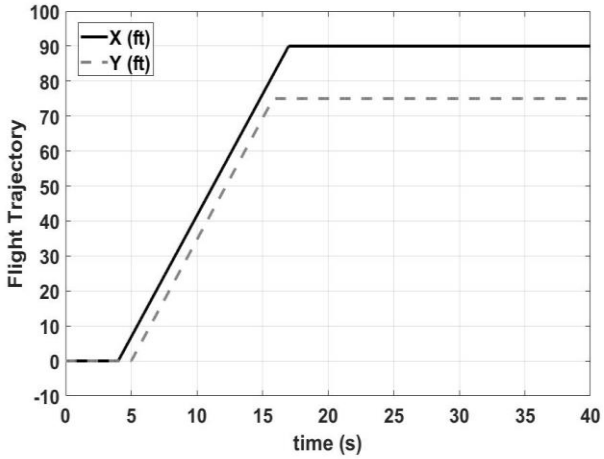

Fig. 17 Hover task flight trajectory command

The commanded task was to initiate the maneuver from the stabilized hover condition, at a suitable reference altitude (approximately 20 ft.), translate longitudinally 90 ft. and laterally 75 ft. at a ground speed of between 6 and 10 kts and return to a stabilized hover, maintaining the desired heading deviations throughout the maneuver [22]. The ADS-33E-PRF task performance requirements are described in Table 3.

Table 3 ADS-33E-PRF Precision Hover task criteria [22]

Criteria	Desired	Adequate
Attain stabilized hover within *X* secs of initiation of deceleration	5	8
Maintain a stabilized hover for at least *X* secs	30	30
Maintain the longitudinal and lateral position within ±*X* feet.	3	6
Maintain heading within ±*X*°	5	10

Figure 18 shows the task performance responses obtained from the SIMSHOL tool for the two simulation setups; with the ideal flight trajectory command using originally designed pilot gains (black dashed line), and with the HELIFLIGHT-R piloted simulation flight trial trajectory command using optimized pilot gains (red dashed line) obtained using proposed response optimization technique, compared with the PSFT results. The desired task requirements illustrated in Table 3 were successfully achieved by the tool showing an overall good agreement. However, from the response of the non-optimized condition, it appears that the pilot model loop gains obtained in the previous section needed tuning in the linear velocity loops to further improve the match. Another reason for the slight disagreement is because the SIMSHOL was commanded with an ideal Precision Hover task flight trajectory shown in Fig. 17. Thus, for the purpose of testing the ability of the tool to reproduce responses similar to that of a real pilot in the simulator, the SIMSHOL was commanded with the piloted flight trajectory obtained from the PSFT performed in the HELIFLIGHT-R

simulator. The pilot loop gains were then tuned automatically using the proposed error-minimization based response optimization methodology, detailed in Section VII.

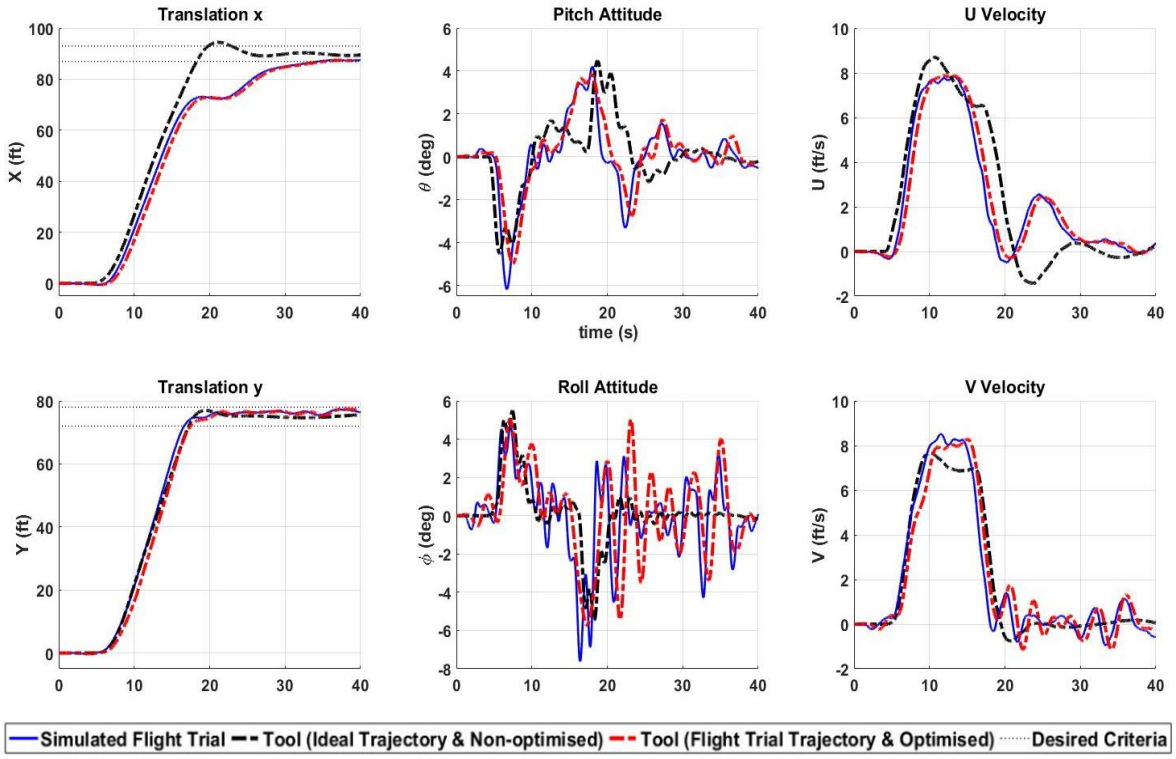

Fig. 18 Comparison of SIMSHOL tool and flight simulation trial responses in Precision Hover task

Within the optimization procedure, the pilot loop gains varied approximately 5 to 15 % from those originally designed in Section IV. The pilot model reproduces the aircraft responses obtained from the piloted simulation trial very well (red dashed line). The structure of the overall pilot loop transfer functions optimization model, optimization procedure steps and its further utilization in obtaining a universal configuration of the SIMSHOL tool are detailed in Section VII.

VI. HSDI Deck Landing Simulation Development

Using the SIMSHOL tool, a HSDI scenario was constructed for simulating the UK standard deck landing task for a SH-60B helicopter to a single-spot destroyer in the presence of a turbulent airwake and with deck motion. The influence of the CFD-generated ship airwake for a 25 kts headwind was included through the application of a representative spatial ship airwake turbulence technique developed in this study. Deck motion was included using a well-validated ship motion modelling software for the ship moving at 12 kts through a seaway of Sea State 4 (SS4). To provide PSFT data, the same simulation environment was developed in the HELIFLIGHT-R simulator and pilot-in-the-loop simulations were carried out by two experienced former Royal Navy (RN) test pilots. The simulation results obtained from SIMSHOL simulations were compared with the PSFTs to analyze the task performance and optimize the tool.

A. Flight Trajectory Task Command Generation

The standard RN procedure for a port-side forward-facing recovery was adopted as the flight trajectory, illustrated in Fig. 19. This technique requires the pilot to guide the helicopter to a hover position alongside the port side of the ship's deck and matching the ship's forward speed, followed by a lateral translation to a hover over the deck spot before descending to land on the flight deck [2]. Four (Mission Task Elements) MTEs were identified from this description of the deck landing mission: (i) approach (ii) sidestep maneuver; (iii) station-keeping above the flight deck; and (iv) vertical landing (touchdown).

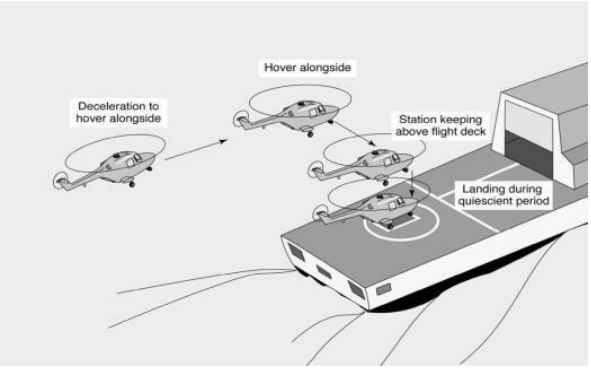

Fig. 19 UK RN standard deck landing approach [2]

The HSDI simulation environment modelled using SIMSHOL consisted of: the low-speed forward flight linearized vehicle model trimmed at 12 kts ground speed with a 13 kts headwind to represent 25 kts headwind WOD airwake condition; ship motion at a 12 kts speed in a SS4 seaway; and an equivalent 25 kts WOD airwake turbulence using the Control Equivalent Turbulence Input (CETI) stochastic model [40,41] modified to capture spatial turbulence intensities from a CFD-computed ship airwake. Figure 20 shows the ship's geometry and simulated MTEs.

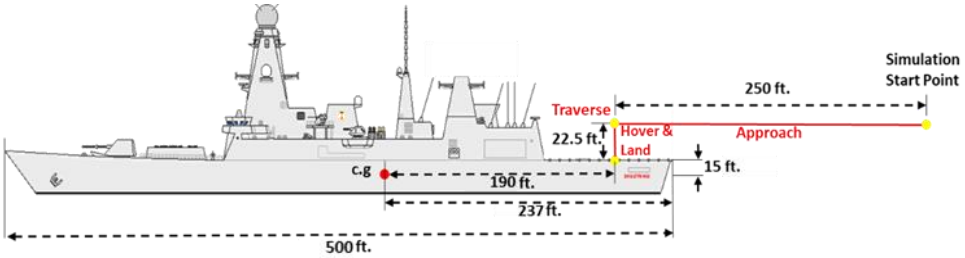

Fig. 20 Single-spot destroyer geometry

The ideal flight trajectory input commanded to the SIMSHOL tool is shown in Fig. 21. The coordinate system is as follows: surge is positive from stern to bow, sway from port to starboard and heave bottom to top. The aircraft was trimmed at the same ground speed as the ship (i.e., 12 kts) and the simulation start location of the aircraft was 250 ft. aft of the ship landing spot, as can be seen from Fig. 20, therefore, to

accomplish/simulate the approach MTE, an initial forward translation command was provided to the aircraft at a constant velocity of 2.77 ft/s for 90 secs to approach alongside the ship's deck and then a trim speed of 12 kts was maintained alongside the ship, see Fig. 21.

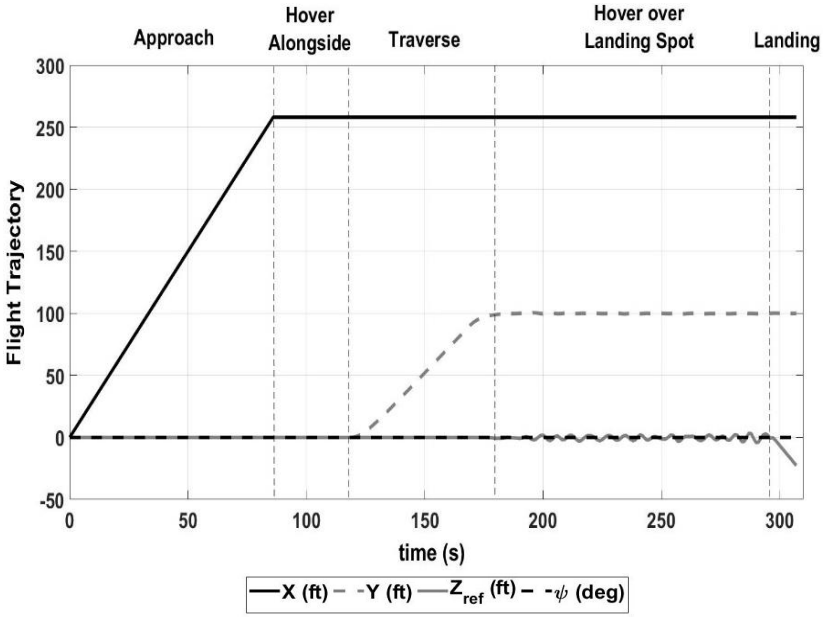

Fig. 21 Flight trajectory input command for HSDI task simulation

B. Ship Motion Modelling (ShipMo3D)

The ship motion was modelled for the corresponding ship and WOD condition using a well-validated ship motion potential-flow modelling code, ShipMo3D, developed at Defence Research and Development Canada (DRDC) – Atlantic [42]. The ship characteristics were: Length 150 m, Beam 17.6 m, Displacement 8,040 t, Draught 6 m, Metacentric height 1.8 m, Number of Panels (wetted hull) 1342, Propeller diameter and rotational speed 4 m and 106.5. RPM (@ 12 kts). To account for the ship motion effect, it was assumed that the helicopter can land safely on the ship's landing deck if the SIMSHOL tool is capable of following its relative position and maintain altitude clearance within the safe boundary for a given time (evaluated in Section VI.D). Therefore, the ship landing deck's lateral and heave motion, shown in Fig. 22, served as a part of the flight trajectory command input to the SIMSHOL in the station-keeping MTE portion, as shown in Fig. 21. SIMSHOL's ability to track the deck motion was examined by the task performance error evaluation, which will be discussed in Section VI.D, Fig. 31. The ship motion was first calculated at the ship's c.g. using ShioMo3D and the landing spot motion was calculated using Eqns. 7 and 8. As can be seen from the equations, the ship landing spot's heave motion is a function of ship's heave, pitching and rolling motion, while ship landing spot's sway motion is a function of ship's sway, heading and rolling motion.

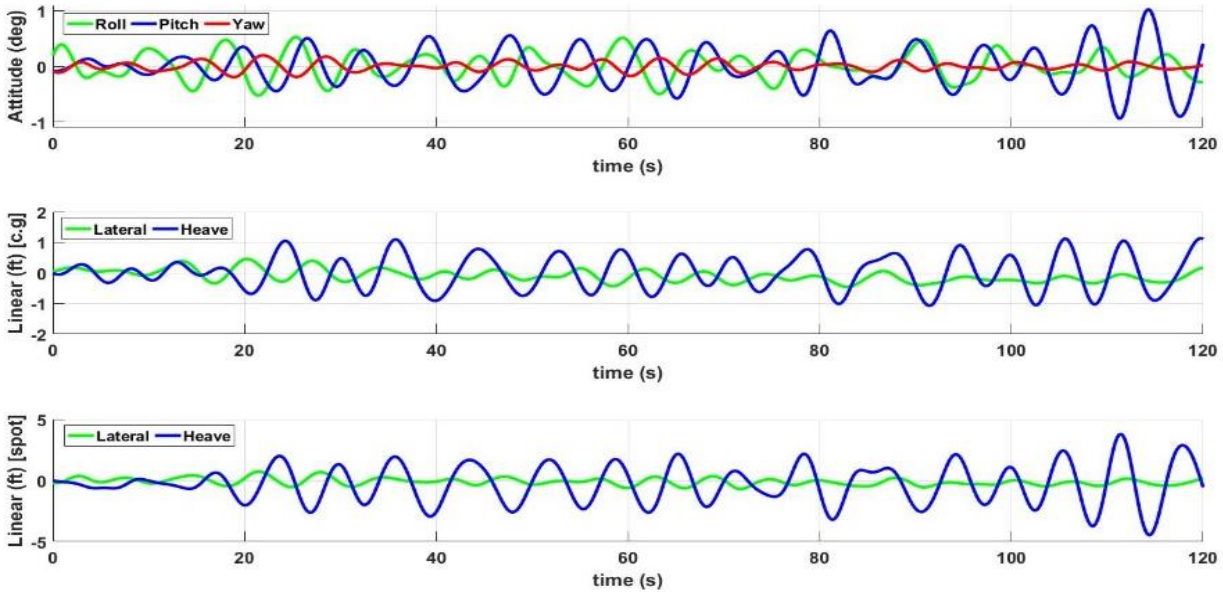

Fig. 22 Single-spot destroyer sea state 4 ship motion at c.g. and landing spot

$$Z_d = Z_{c.g} + \sqrt{X_{l2o}^2 + Z_{l2o}^2}.\sin\theta_s + Z_{l2o}.(1-\cos\phi_s) \quad (7)$$

$$Y_d = Y_{c.g} + X_{l2o}.\sin\psi_s + Z_{l2o}.\sin\phi_s \quad (8)$$

(X_{l2o}, Y_{l2o}, Z_{l2o}) are positions from the ship's landing spot to its c.g. location as shown in Fig. 20 and (ϕ_s, θ_s, ψ_s) are the ship's roll, pitch and yaw attitude. Figure 22 shows the ship motion calculated at a SS4 condition with a 12 kts ship forward speed.

C. Enhanced CFD-Based Spatial Turbulence Integration Methodology

The helicopter in the HSDI environment is immersed in the turbulent airflow over and around the ship's landing deck and superstructure. In addition, there is a further wake created due to the rotor of the helicopter that affects the overall air flowfield. Thus, in reality, there exists an aerodynamic coupling between a helicopter and ship operating in this very dynamic environment [10]. However, generating a complete coupled dynamic system takes excessive time and processing power and is not currently possible in real-time piloted simulations. Therefore, in this study, an enhanced spatial airwake integration methodology has been proposed which integrates a CFD-computed ship airwake within CETI model transfer functions, to capture spatial turbulence intensities along the helicopter flight path in real-time during the SIMSHOL HSDI simulations, representing the UK standard deck landing procedure, see Fig. 23. CETI models the general turbulence field by determining the pilot control inputs that are injected in parallel to the actual control inputs within the SIMSHOL thus producing the spectral characteristics of the aircraft responses representative of that produced in the atmospheric turbulence field. Originally, the identification of the CETI model was

performed by Lusardi et al. [40,41] using a UH-60 helicopter hovering in the turbulent air downstream of a large cubical hangar, which is similar to a deck landing HSDI condition.

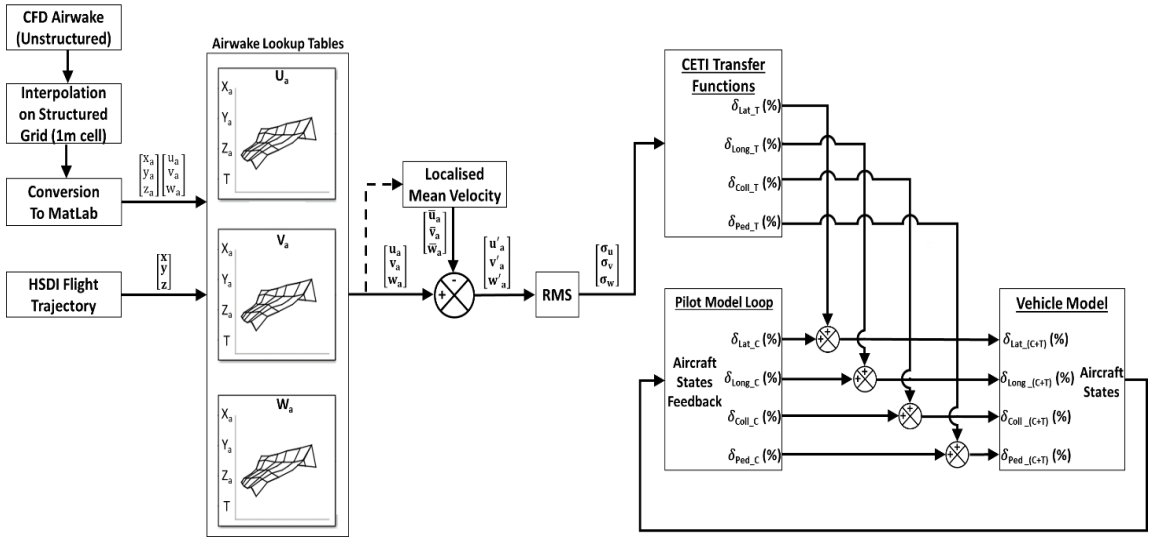

Fig. 23 Proposed spatial CFD airwake integration methodology (An enhanced spatial CETI model)

The CETI model is parameterized by turbulence intensities 'σ', freestream wind velocity 'U_∞', main rotor radius 'R_m' and tail rotor radius 'R_t'. The SH-60B helicopter main and tail rotor radii are 26.85 ft and 5.5 ft, respectively. The generic CETI model was obtained from the Comprehensive Identification from Frequency Responses (CIFER) tool [43]. The white-noise (w_n) driven CETI model transfer functions are given in Eqns. (9)-(12).

$$\frac{\delta_{\mathrm{Lat}}}{w_{\mathrm{n}}} = 0.837\sigma_{\mathrm{w}}(\mathrm{t})^{-0.6265}\sqrt{\frac{\sigma^2 \mathrm{U}_\infty}{\pi \mathrm{R}_{\mathrm{m}}}}\left[\frac{1}{\mathrm{s}+(2\mathrm{U}_\infty/\mathrm{R}_{\mathrm{m}})}\right] \tag{9}$$

$$\frac{\delta_{\mathrm{Long}}}{w_{\mathrm{n}}} = 1.702\sigma_{\mathrm{w}}(\mathrm{t})^{-0.6265}\sqrt{\frac{\sigma^2 \mathrm{U}_\infty}{\pi \mathrm{R}_{\mathrm{m}}}}\left[\frac{1}{\mathrm{s}+(2\mathrm{U}_\infty/\mathrm{R}_{\mathrm{m}})}\right] \tag{10}$$

$$\frac{\delta_{\mathrm{Coll}}}{w_{\mathrm{n}}} = 0.1486\sigma_{\mathrm{w}}(\mathrm{t})^{-0.7069}\sqrt{\frac{3\sigma^2 \mathrm{U}_\infty}{\pi \mathrm{R}_{\mathrm{m}}}}\left[\frac{\mathrm{s}+33.91(\mathrm{U}_\infty/\mathrm{R}_{\mathrm{m}})}{[\mathrm{s}+1.46(\mathrm{U}_\infty/\mathrm{R}_{\mathrm{m}})][\mathrm{s}+9.45(\mathrm{U}_\infty/\mathrm{R}_{\mathrm{m}})]}\right] \tag{11}$$

$$\frac{\delta_{\mathrm{Ped}}}{w_{\mathrm{n}}} = 1.573\sigma_{\mathrm{v}}(\mathrm{t})^{-0.6493}\sqrt{\frac{\sigma^2 \mathrm{U}_\infty}{\pi \mathrm{R}_{\mathrm{t}}}}\left[\frac{1}{\mathrm{s}+(\mathrm{U}_\infty/\mathrm{R}_{\mathrm{t}})}\right] \tag{12}$$

The CETI model would produce a constant turbulence intensity flowfield based on a single turbulence intensity RMS value input to the transfer functions illustrated in the above equations. The output of the CETI model for a local hover point is shown in Fig. 24 in which the CETI output represents a constant turbulence intensity. However, to represent the spatial variation of turbulence around the ship's flight deck, and therefore improve the fidelity of the airwake disturbance modelling, in the enhanced CETI model CFD-computed unsteady airwake data for a 25 kts H00 WOD condition was stored in the 3D lookup tables

consisting of the full structured airwake domain (see Fig. 25), sampled at 25 Hz and interpolated onto a 1 m cell spacing.

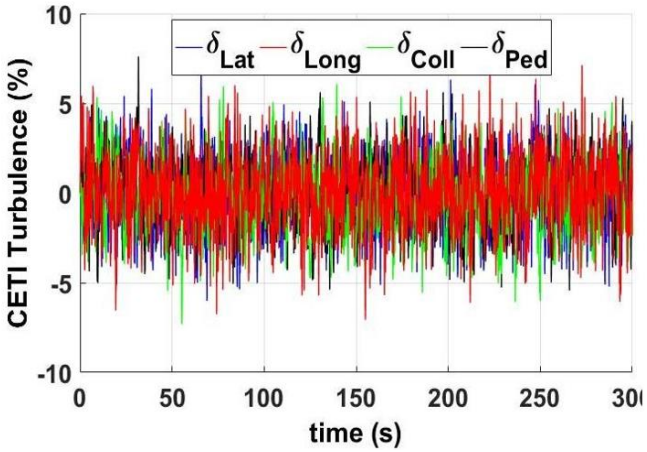

Fig. 24 Original CETI output (localized turbulence)

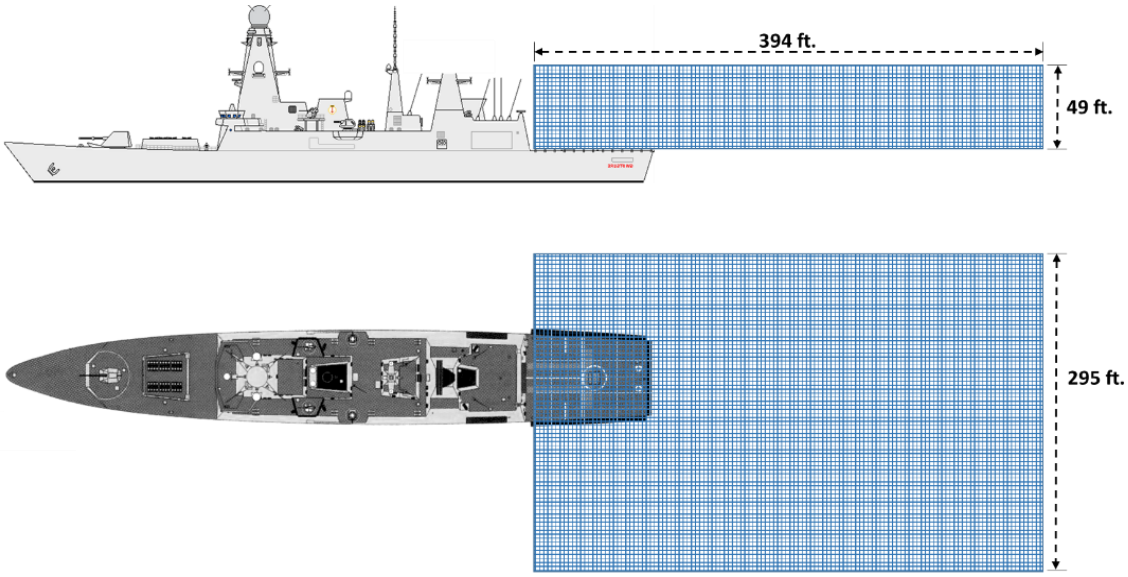

Fig. 25 Ship airwake structured domain

The lookup table maps the location coordinates (x_a, y_a, z_a) of an airwake domain as input to airwake velocity components (u_a, v_a, w_a) stored into it as output. The position of the aircraft relative to the touchdown point on the ship landing deck was used to extract airwake velocity data from the lookup tables, see Fig. 23. Following that, the RMS of the velocity components at every point along the flight trajectory path, as shown in Fig. 26, were calculated and used as an input into the CETI transfer functions, hence modifying the original model into an enhanced spatial CETI turbulence to represent the varying turbulence field around the ship.

Figure 26 shows the spatial variation of the RMS turbulence intensities throughout HSDI MTE phases:

approach, traverse, hover and landing, as specified in Fig. 19. Figure 27 shows the final output produced from the enhanced spatial CETI turbulence model for the turbulence intensities specified in Fig. 26. The turbulence is lowest in the approach MTE since it is outside of the ship's airwake. The RMS values start to increase in the traverse MTE where the aircraft laterally approaches to the deck, encountering the turbulent airwake. Finally, the constant value in the hover MTE corresponds to a single spot in the airwake space, followed by the landing MTE which shows variations until touchdown. The "baseline" CETI model is not capable of representing the turbulence field in the approach, traverse and landing MTEs of the standard deck landing procedure where the turbulence intensity varies along the flight path, whereas the modified turbulence model does capture the spatial variation of turbulence intensities in real-time from the time-accurate unsteady CFD airwake over and around the ship landing deck and superstructure.

For modelling an air flowfield environment, there exists a standard approximate ratio [24,28] (Eqn. (13)) between ambient wind speed 'U_∞', mean wind speed at the landing spot 'U_L' and the total turbulence intensity at that point 'σ_T'. Eqn. (14) specifies the ratio of the condition simulated in this paper.

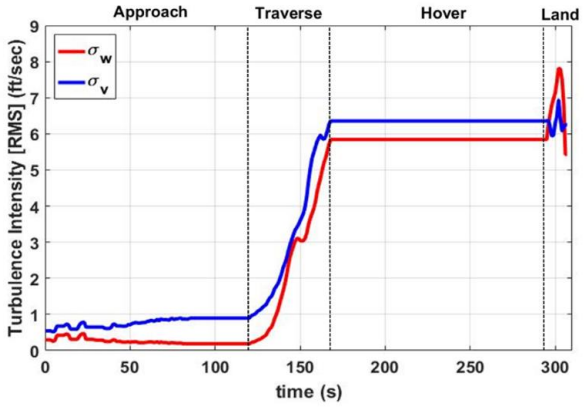

Fig. 26 Turbulence Intensities along HSDI flight Path

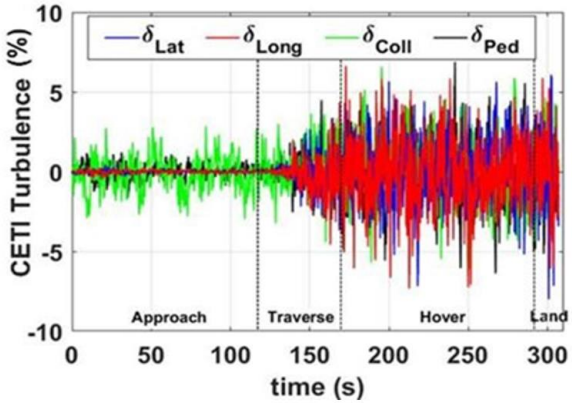

Fig. 27 Enhanced spatial CETI model output

$$U_\infty : U_L : \sigma_T = 1:0.4 \sim 0.58:0.05 \sim 0.13 \text{ (standard)} \quad (13)$$

$$U_\infty : U_L : \sigma_T = 1:0.51:0.14 \text{ [42.2:21.5:6.2 ft/s] (in this case)} \quad (14)$$

The SIMULINK final form of the SIMSHOL tool is presented in Fig. 28, which shows the flight trajectory command input, enhanced CETI airwake model, pilot model loops, vehicle dynamic model and a 3D visualization of the simulation output.

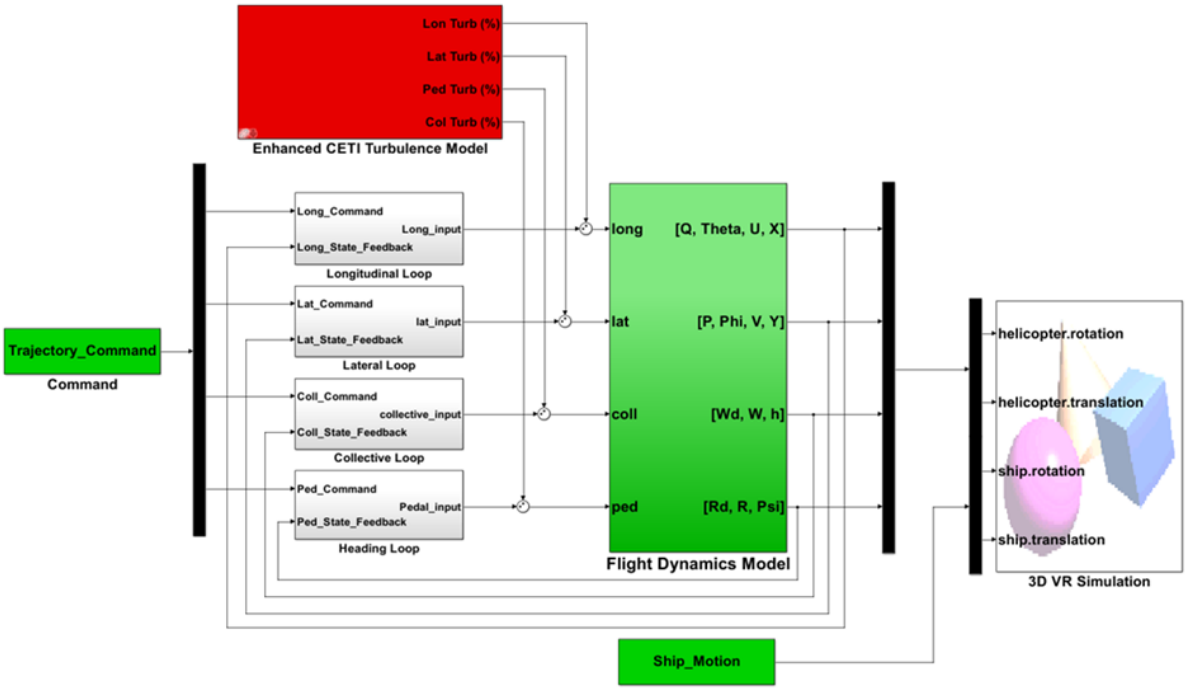

Fig. 28 SIMULINK SIMSHOL predictive simulation tool model

D. Simulation Results

A number of deck landings were simulated using the developed SIMSHOL tool. Figure 29 shows the results of the tool primarily tracking the position of the landing spot, with and without the enhanced spatial CETI airwake, for the station-keeping hover MTE. The hover MTE simulation starts at a stationary position 22.5 ft above the landing spot (i.e., approximately at ship's hangar height), illustrated earlier in Figs. 20 and 21. It can be seen in Fig. 29 that, with and without the airwake, the SIMSHOL tool tracks the ship's heave and sway motion well and maintains sufficient altitude clearance from the ship's landing deck. It can further be seen that the enhanced airwake CETI turbulence has a noticeable disturbance effect on the response of the helicopter, especially in attitude. However, the tool successfully accomplishes the task, rejecting the external disturbances whilst maintaining the desired position.

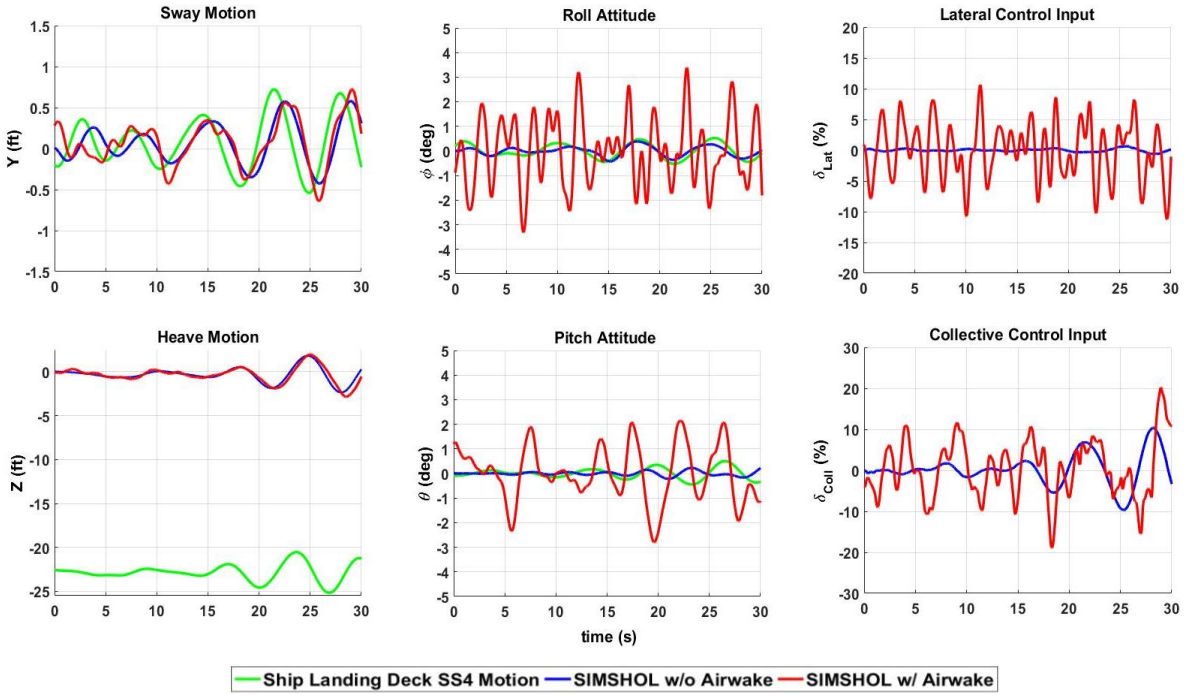

Fig. 29 SIMSHOL HSDI Simulation Results for a 30 sec hover

Figure 30 shows the control inputs (red lines) and the enhanced spatial CETI model's output (blue lines) simulated by the SIMSHOL tool, throughout the task in all four MTEs of the standard deck landing procedure. During the approach and port-side hover MTE, forward longitudinal cyclic control input is applied at t=0 secs to initiate the forward translation command and at t=88 secs the stick is pulled back to finish the approach MTE. No change in command is input to the SIMSHOL for the next 30 secs and the aircraft maintains forward flight at ground trim speed alongside the port-side of the landing deck before starting the traverse MTE. Since the aircraft experiences lowest turbulence in the approach MTE, the stick deflections and spatial CETI turbulence are both small. To initiate the traverse MTE, lateral control stick input is applied

at *t*=119 secs to translate the aircraft laterally to the ship's landing deck while the forward flight is maintained. During this MTE the aircraft encounters the turbulence produced by the ship's superstructure, as illustrated earlier in Fig. 26. As the turbulence increases alongside, the control compensation increases as well to counteract the disturbances. This maneuver finishes at *t*=175 secs over the landing spot. During the hover MTE, the aircraft is commanded to track the sway and heave motion of the ship's landing deck while rejecting the disturbances and maintaining sufficient altitude clearance and forward flight at ground trim speed. It can be seen that the turbulence and the control activity in all four axes during the hover MTE are higher throughout this phase. Finally, the landing MTE is initiated with the collective lever input at *t*=295 secs when the heave motion of the ship's landing deck is minimum, using a simple relative deck position logic.

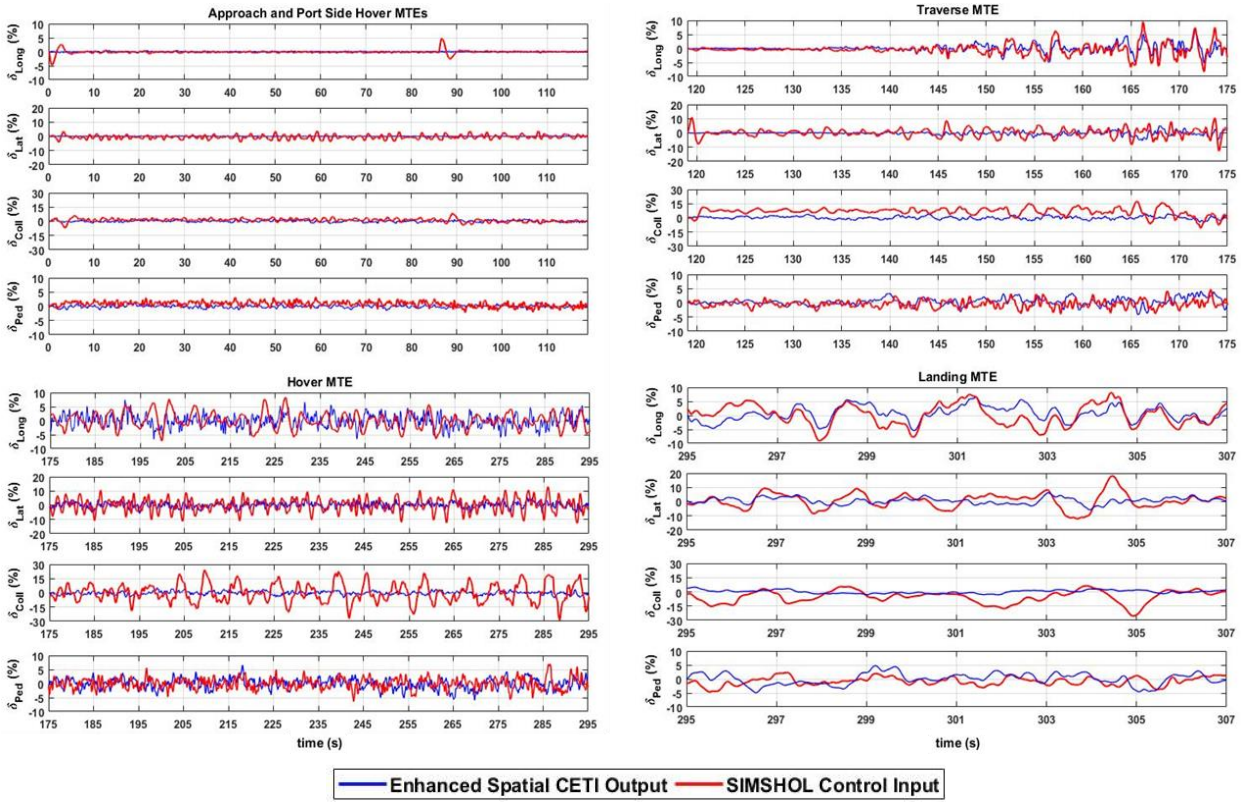

Fig. 30 SIMSHOL stick control and Enhanced Spatial CETI output time histories (trimmed reference)

To evaluate the performance of the station-keeping MTE of the overall HSDI task, the task performance can be quantified by determining the position tracking errors [28]. Figure 31 presents the tracking errors evaluated from one of the simulation runs, which shows that the calculated position errors (ship deck movement minus aircraft movement) are well within the desired task performance criteria as specified in [28] for a similar dynamic interface task, and listed in Table 4. The aircraft is expected to remain within a rectangular box throughout the tracking/hover MTE.

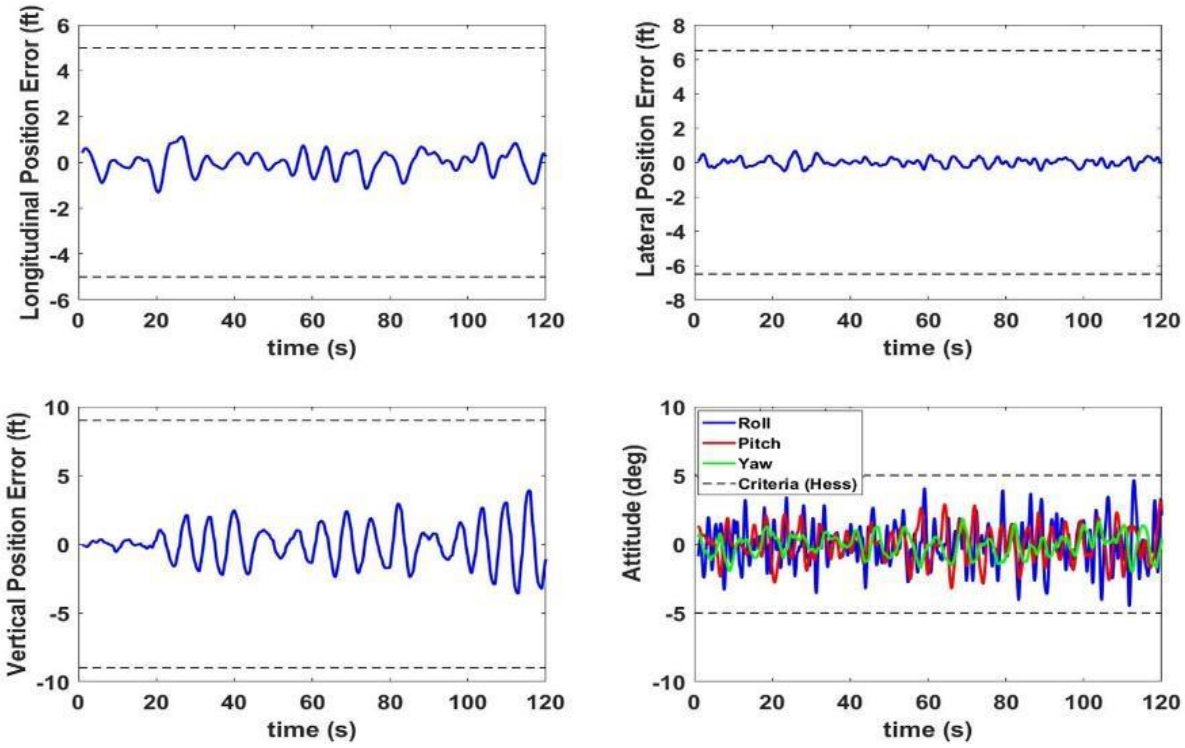

Fig. 31 SIMSHOL performance evaluation through tracking errors

Table 4 HSDI position tracking task performance criteria [28]

Performance	X	Y	Z	Attitude
Desired	±5 ft.	±6.5 ft.	±9.5 ft.	±5°
Adequate	±6.5 ft.	±9.5 ft.	±13 ft.	±10°

To further analyze SIMSHOL's performance, Fig. 32 compares the FFTs of the piloted simulation flight trial and SIMSHOL for roll, pitch, and yaw rate responses during the station-keeping MTE. Figure 33 compares the Bode plots identified from the piloted simulation flight trial and SIMSHOL HSDI responses in the station-keeping MTE. Three on-axis conditions are compared: roll rate response to lateral control input, pitch rate response to longitudinal control input, and yaw rate response to pedal input. It can be seen that SIMSHOL predicts the responses reasonably well throughout the frequency range.

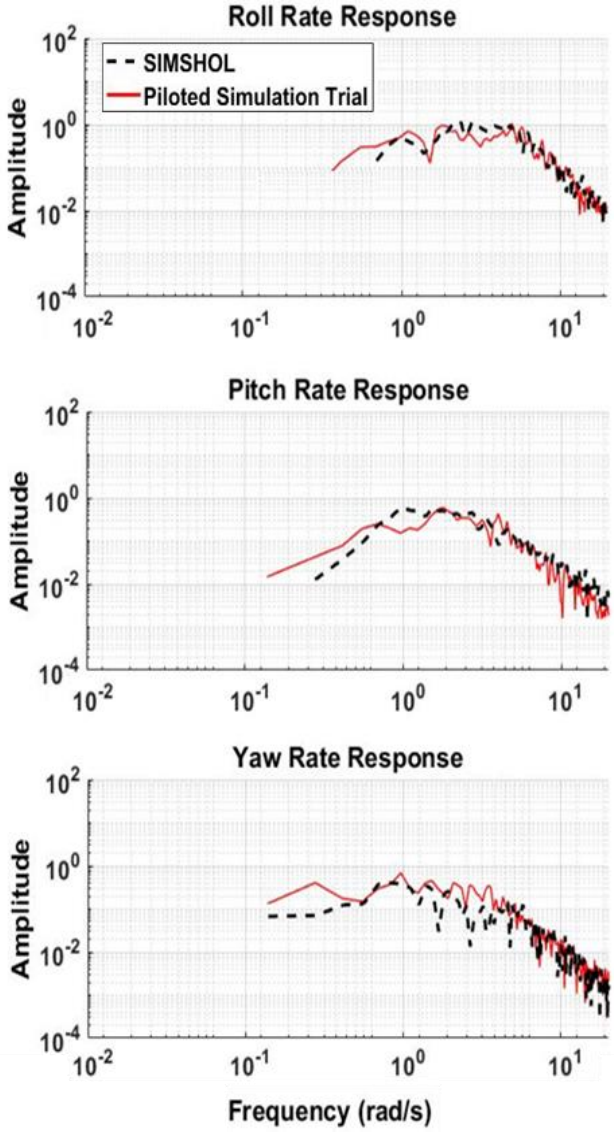

Fig. 32 Attitude rate response FFT comparison

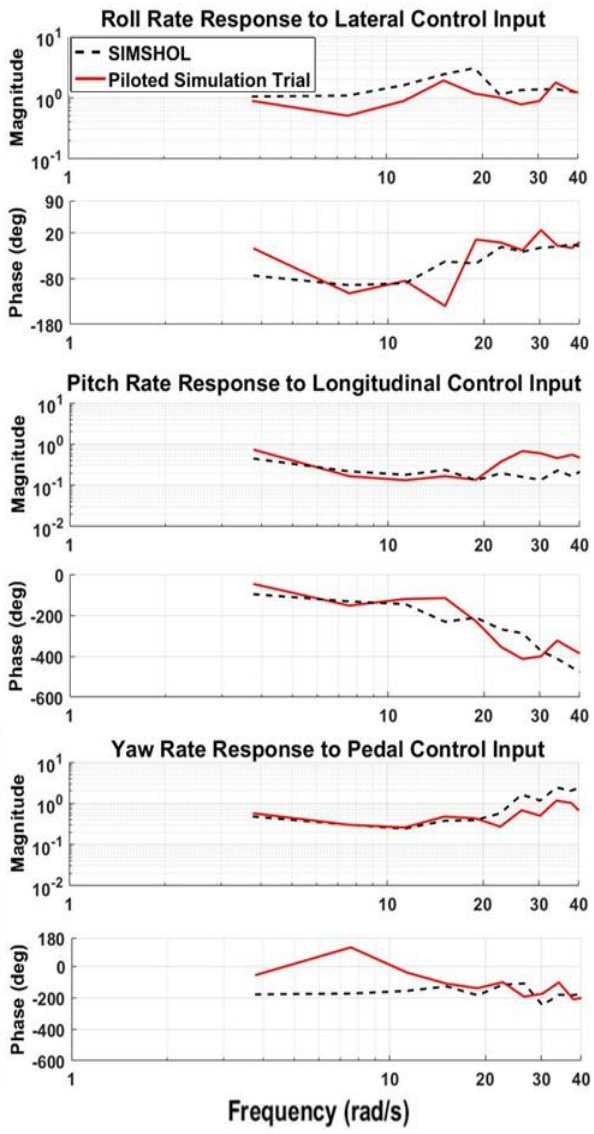

Fig. 33 On-axis identified bode plots comparison

The overall agreement between PSFTs and SIMSHOL is good throughout the frequency range. As demonstrated in Fig. 31, the tool was capable of accomplishing the task well within the task performance criteria shown in Table 4, successfully rejecting the airwake disturbances while tracking the moving deck. Moreover, the enhanced spatial CETI model which has been developed, simulates the particular HSDI turbulence effect reasonably well, representing the real-world challenging deck landing condition. However, as demonstrated in the Precision Hover task in Section V, the SIMSHOL response can be further improved by utilizing the PSFTs data using the response optimization technique; therefore, the pilot loop gains were optimally and objectively tuned for this case as well to obtain an optimized setting of the tool for high-fidelity task simulation performance, detailed in the following Section.

VII. Response Optimization Methodology

To optimize the SIMSHOL tool for high-fidelity HSDI offline task simulations to be performed as closely and accurately as possible to the real-human pilot's performance in the simulator, a task-specific objective response optimization methodology was formulated within MATLAB's Design Optimization program function [44], using a historical database of numerous piloted flight trials in the HELIFLIGHT-R simulator. The optimizer model applied was the iterative Gradient Descent method set to use the Sequential Quadratic Programming algorithm devised with PSFT vs SIMSHOL responses RMS error minimization problem function as an optimization objective. The model was used to automatically optimize the pilot model sequential loop transfer function gains for the low speed forward flight condition (H00 25 kts WOD case) which were initially designed using F-T and T-D criteria in Section IV and employed here as a baseline for initialization of the optimization iterations, as performed in Section V for the ADS-33 Precision Hover task. The purpose of the proposed methodology was to assess the limit to which the SIMSHOL's response could be improved, and to train the SIMSHOL tool for it to be used in the future for simulated SHOL predictions prior to FOCFTs. Moreover, the intention was to obtain a universal set of optimized pilot model loop gains which can potentially be used in the SIMSHOL tool for the range of helicopter-ship combinations at the same WOD airwake condition, so that for every different combination the gains need not be updated.

PSFTs data were obtained from the HELIFLIGHT-R database for SH-60B helicopter landings on five different ships by two former RN test pilots. The ships were the Queen Elizabeth class aircraft carrier (QEC), Wave class auxiliary oiler, a destroyer similar to the UK's Type 45 Daring class, Simple Frigate Shape v2 (SFS2), and a UK Duke class Type 23 frigate [3,10,13,15,19,20]. Piloted simulation flight trajectories flown by the test pilots from each of the helicopter-ship combination trials were used as input to SIMSHOL trajectory block, instead of ideal flight trajectories shown earlier in Fig. 21. The SIMSHOL responses obtained from the tool were compared with the responses of the PSFTs to reduce the error between them by automatic tuning of the pilot model loop transfer function gains in each axis using the proposed optimization method.

The steps below explain the optimization process configured to first optimize SIMSHOL's performance and subsequently derive an optimal set of pilot model loop gains at which SIMSHOL's response is closest to the PSFT results. The objective of the optimization loop is to compare the SIMSHOL simulations with the PSFTs performed by the real-human pilot for a particular test case and minimize the RMS error between the aircraft states using the devised iterative optimization algorithm, which varies the pilot model loop gains iteratively until the optimal set of gains are obtained at which the RMS error is minimum. The optimization structure is shown in Fig. 34.

i. Modify the pilot model loop for the SIMSHOL response comparison with the PSFT data. Input PSFT trajectory command as an input to SIMSHOL flight path trajectory command generator loop.
ii. Specify baseline/artificially designed pilot loop gains for the initialization of optimization iterations as optimization design variables and define a suitable maximum and minimum range of design variables

variation during the optimizer iterations. All fourteen sequential model loop gains are added in the optimization problem as design variables.

iii. Specify the PSFT-SIMSHOL responses RMSE output signal within the modified pilot model loop to be logged as an optimization function criterion that is to be minimized.

iv. Form the minimization problem function script for each axis within each channel (Lateral, Longitudinal, Collective and Pedal).

v. When the SIMSHOL optimization simulation is run for the baseline configuration of the pilot loop transfer functions the RMS error signal specified is logged and used by the algorithm in the evaluation of the design requirements for the next iteration to minimize the function output (i.e., RMS error comparison signal).

vi. The algorithm produces the new set of tuned pilot model loop gains which are uploaded to SIMSHOL to replace the previous set and the simulation is run again automatically. The RMS error between SIMSHOL and PSFTs' responses (aircraft states) is compared to determine if the optimization solution (i.e., gradient descent) has converged with 0.001 constrained tolerance and function output has been minimized.

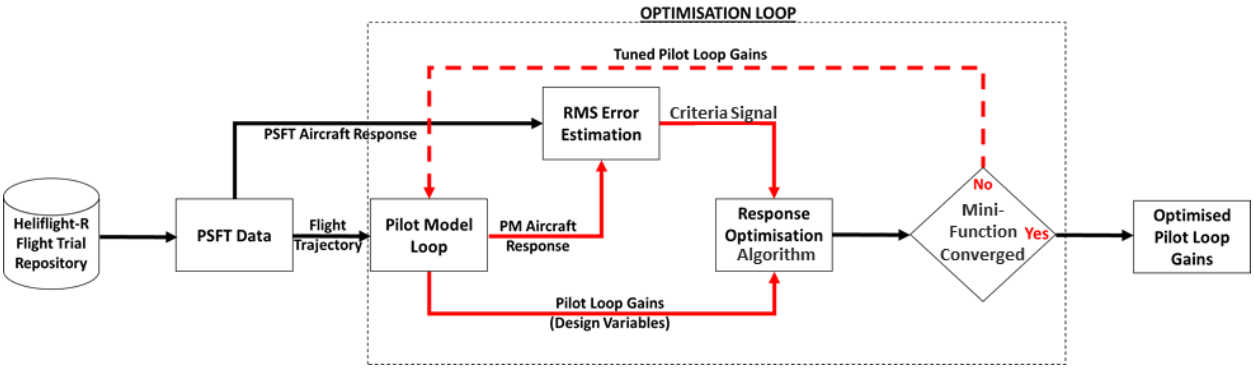

Fig. 34 Proposed SIMSHOL automatic response optimization model structure

Initially, the optimization methodology was applied to obtain an optimized set of gains for the landings on the single spot Destroyer to progress with the simulations performed in Section VI. Subsequently, using the optimized set of gains, simulated landing operations on five different ships of different size, shape, and configurations were examined (see Fig. 35) for a 25 kts headwind WOD using the response optimization model, and a single universal set of pilot loop gains was designed which provided optimized aircraft responses for landing tasks on all five ships. Figures 36 to 40 show good agreement between the optimized spectral (periodograms) responses from SIMSHOL compared to the PSFTs for landings for the ships mentioned above.

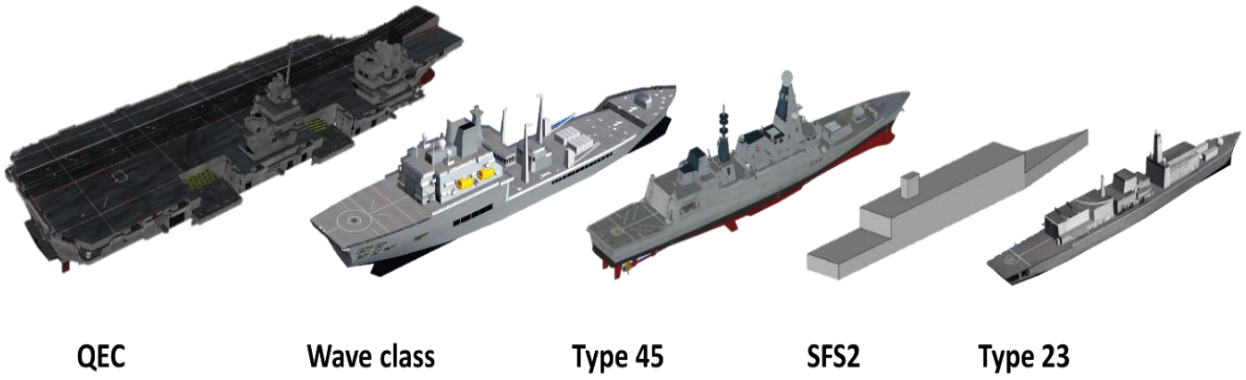

Fig. 35 Ships used for HSDI simulations: QEC (280 m); Wave Class Oiler (196 m); Type 45 'Like' (152 m); SFS2 (139 m); Type 23 Frigate (133 m)

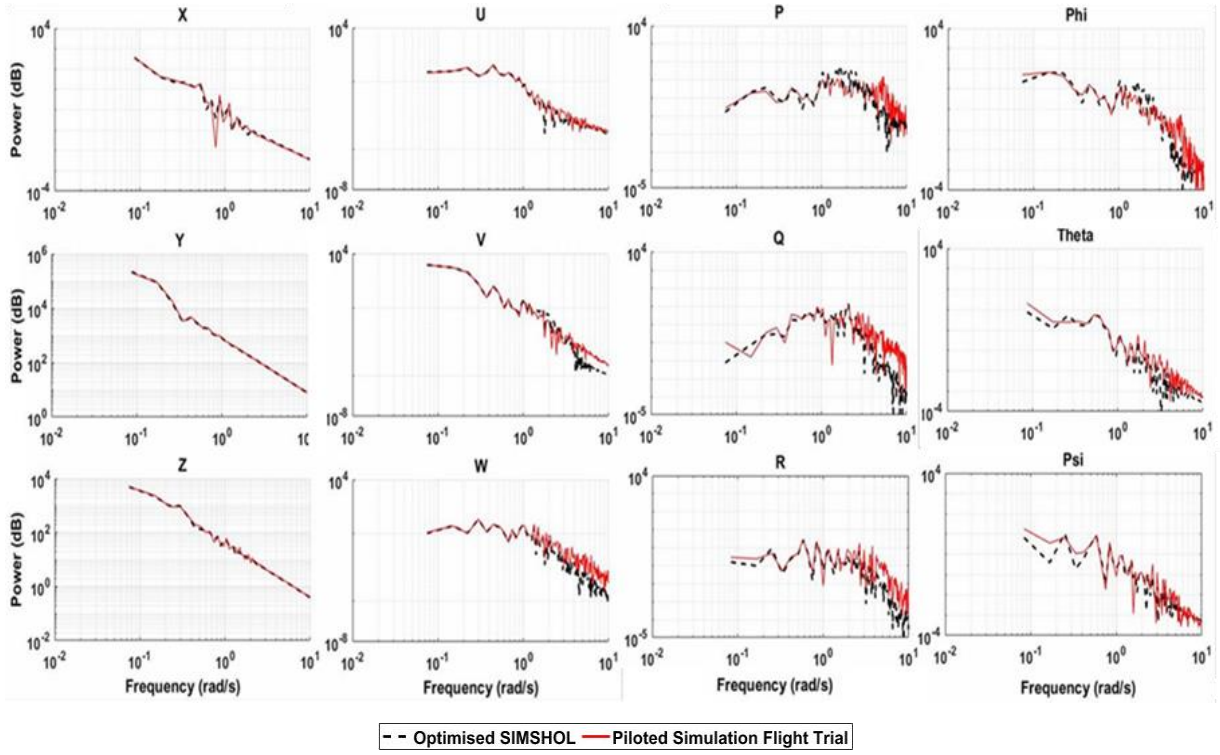

Fig. 36 Comparison of PSDs of SIMSHOL and PSFT for QEC deck landing task

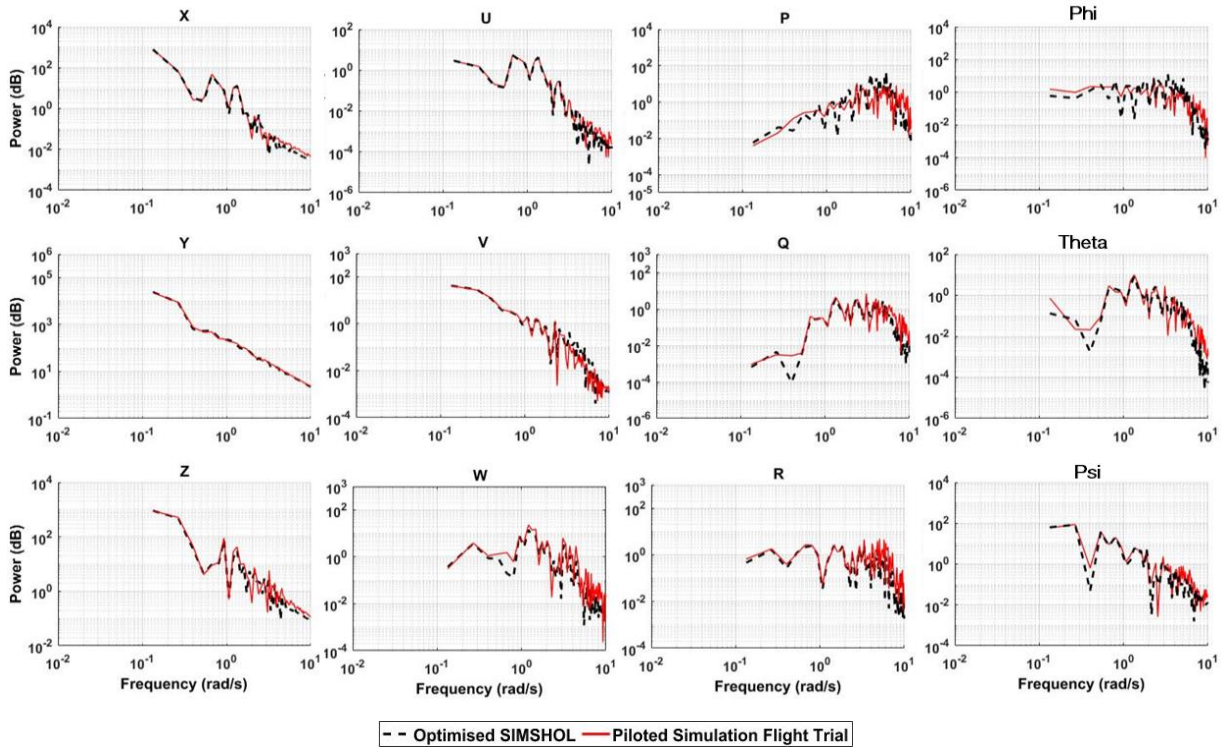

Fig. 37 Comparison of PSDs of SIMSHOL and PSFT for Wave Class Auxiliary Oiler deck landing task

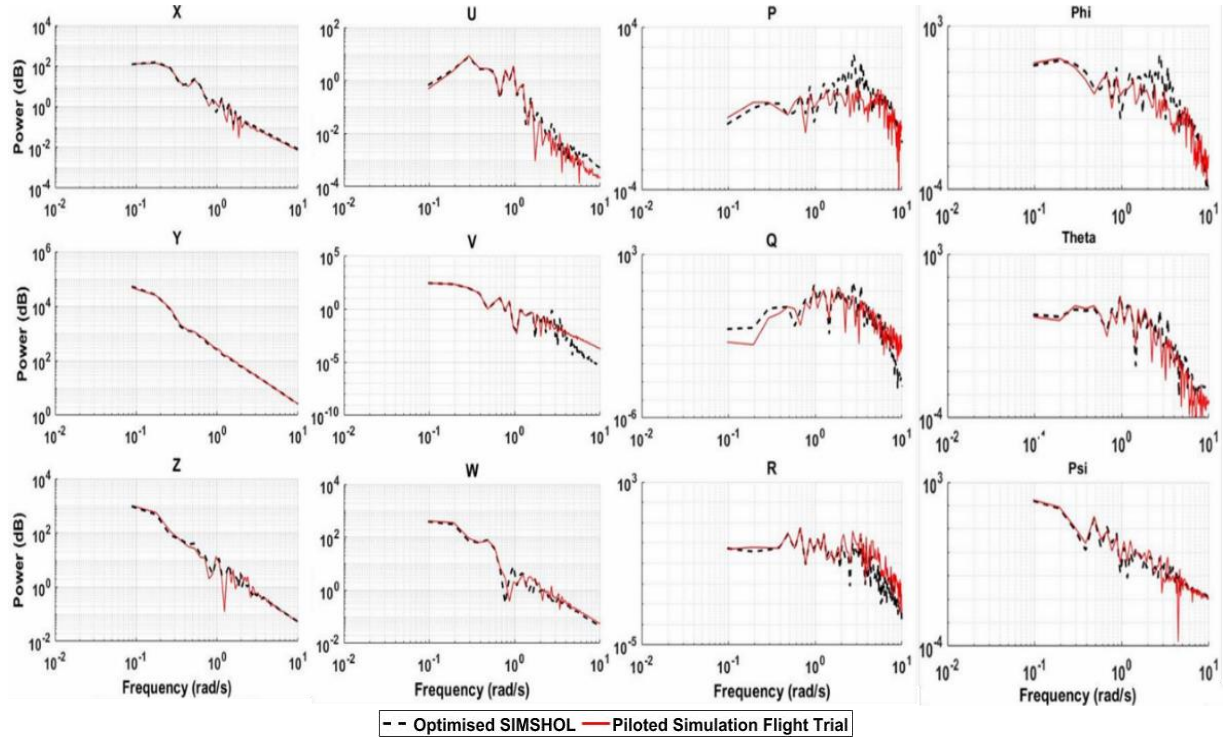

Fig. 38 Comparison of PSDs of SIMSHOL and PSFT for T45 destroyer deck landing task

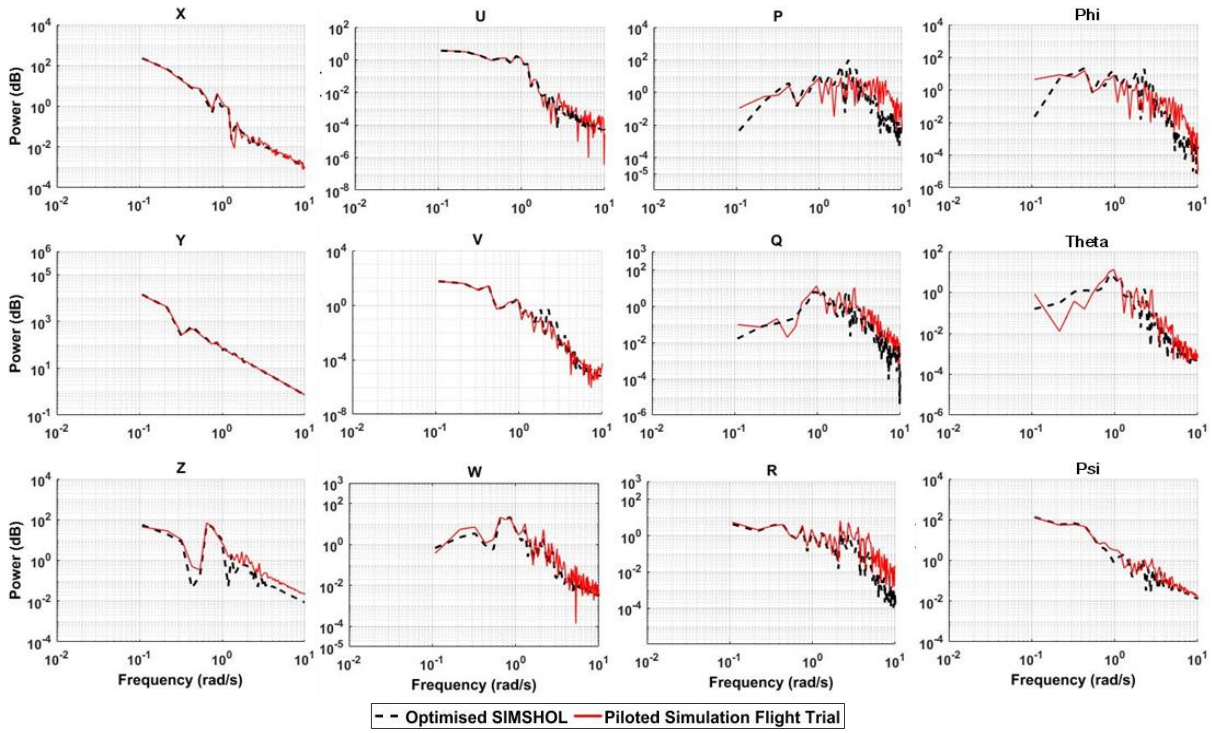

Fig. 39 Comparison of PSDs of SIMSHOL and PSFT for SFS2 deck landing task

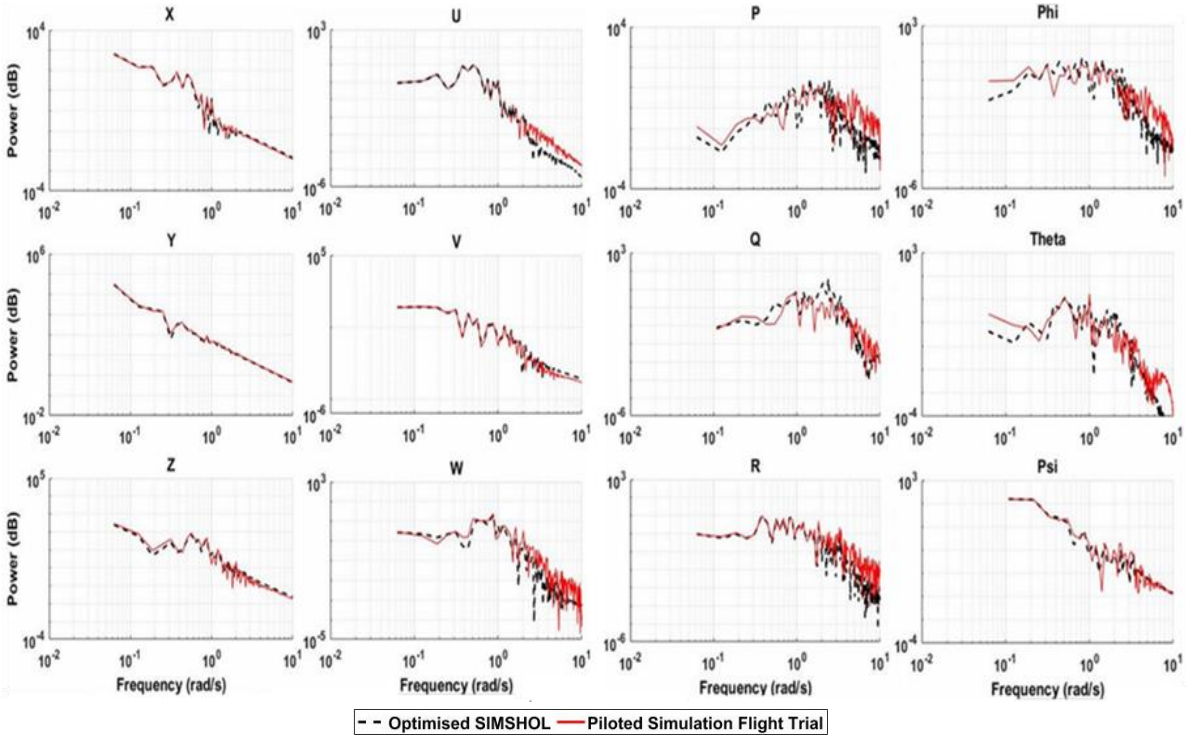

Fig. 40 Comparison of PSDs of SIMSHOL and PSFT for T23 Frigate deck landing task

VIII. Conclusions

The research presented in this paper has been aimed at developing a high-fidelity desktop-based simulation tool which predicts piloted helicopter landing on the deck of a moving ship in the presence of a turbulent airwake and deck motion. The developed tool models the pilot, vehicle, task, and environment elements and has been compared with equivalent piloted deck landings conducted in a full-motion flight simulator. The simulation tool has been called SIMSHOL and the paper has described how the tool has been developed and applied to a number of helicopter-ship combinations at a particular WOD condition. The overall aim has been to construct a high-fidelity optimized simulation framework which, compared with at-sea trials, offers a faster, cheaper, and more efficient method of assessing the difficulty of landing a helicopter to a ship. The following are the key conclusions drawn from this work:

1. In the initial pre-validation phase of the SIMSHOL tool, in which ADS-33E-PRF Precision Hover task was simulated, the tool was shown to be suitable for offline desktop-based task simulations and analysis.
2. An objective response optimization technique was developed to improve the Precision Hover task performance by objective pilot model loop transfer function tuning using PSFTs data. Using the response optimization methodology, the gains of the pilot model loop transfer functions were tuned to derive an optimized set of gains which improved the response match between SIMSHOL and the PSFT, representing a pilot's performance in the simulator.
3. An enhanced spatial CETI turbulence integration technique has been developed, and applied within SIMSHOL, to capture the spatial variation of turbulence intensities over and around the ship's landing deck along the desired flight trajectory path in real-time during SIMSHOL simulations. The modified CETI model utilizes CFD-generated ship airwake data to provide the spatial variation of the turbulence intensities along the flight path throughout the different phases of the standard deck landing procedure.
4. The tool was further developed by constructing and simulating the HSDI environment for a 25 kts headwind WOD airwake condition. It was found that in the critical station-keeping MTE simulation, the SIMSHOL tool was capable of maintaining the desired helicopter clearance from the ship's landing deck and superstructure while tracking its lateral and vertical motion, thus rejecting the external airwake disturbances and accomplishing the deck landing task successfully within specified task performance metrics.
5. A piloted simulation trial was conducted in the HELIFLIGHT-R simulator for the same HSDI condition (i.e., SH-60B landings on a single-spot destroyer) to compare, validate and optimize the SIMSHOL tool to be able to predict deck landing performance as close as possible to the real human pilot. After simulating the HSDI conditions within the SIMSHOL tool and performing several deck landings, time and frequency domain comparisons of the SIMSHOL with PSFT responses were examined and showed good agreement. Subsequently, the response optimization technique was used to optimize the HSDI task simulation performance.

6. An error-minimization based Response Optimization methodology was further developed and integrated with the SIMSHOL tool. A database of HELIFLIGHT-R flight trials was used to automatically optimize the pilot model transfer functions and train the tool to predict deck landing performances by better representing a real pilot's behavior in the simulator. A universal configuration of the tool was obtained by examining the SIMSHOL deck landing simulations on five different naval ships and comparing them with PSFTs, which led to the derivation of an optimized set of pilot loop gains capable of predicting limits with a high level of confidence for all five combinations. The frequency domain comparisons of the PSFTs with SIMSHOL showed good agreement for all the helicopter-ship combinations.

Using the SIMSHOL tool, and comparing with PSFTs, it has been found that it is capable of representing the HSDI pilot-vehicle-task-environment system within acceptable boundaries and it possesses potential to be used as a PSFTs planning and preliminary task investigation tool to inform and support real-world FOCFTs. In the final phase of the tool's development, it is intended to integrate the tool within the FLIGHTLAB environment where the full-scale non-linear vehicle model will be utilized along with the full interaction of the CFD-generated ship airwake influencing the flying qualities of the simulated helicopter based on Airload Computation Points Method (ACPs) distributed around the helicopter rotors, empennage and fuselage. Airwakes and ship motion for different wind speeds and directions can also be incorporated. Moreover, it is intended to perform a three-point comparative assessment between SIMSHOL, PSFTs, and FOCFTs to develop a workload metric to be able to further enhance the tool's fidelity and to efficiently predict preliminary simulated SHOL envelopes.

Finally, it is well understood that the tool is not offered as a substitute for piloted flight trials, it is intended for it to be used in conjunction with piloted simulations and real-world flight trials to quicken the process of deriving ship-helicopter operating limits.

Acknowledgements

The authors would like to thank the industrial sponsors, QinetiQ and Dstl for funding the project under QinetiQ-Dstl Technology Fund (award no. CON-566). The authors would also like to thank: Dr Sarah Scott, a former researcher at the University of Liverpool, for access to the Type 45 ship airwake data and the former RN test pilots who conducted the simulation flight trials.

References

[1] Lumsden, B., Wilkinson, C. H., and Padfield, G. D., "Challenges at the Helicopter-Ship Dynamic Interface," *24th European Rotorcraft Forum*, Marseilles, France, Sep. 1998, pp. 1-23.

[2] Fang, R., Krijns, H. W., and Finch, R. S., "Dutch/British Clearance Process," RTO AGARDograph 300: Helicopter/Ship Qualification Testing, edited by G. D. Carico, R. Fang, R. Finch, W. P. Geyer, Jr., H.W. Krijns, and K. Long, Vol. 22, Flight Test Techniques Series, NATO Research and Technology Organization, 2003.

[3] Forrest, J. S., Owen, I., Padfield, G. D., and Hodge, S. J., "Ship-Helicopter Operating Limits Prediction

Using Piloted Flight Simulation and Time-Accurate Airwakes," *Journal of Aircraft*, Vol. 49, No. 4, June 2012, pp. 1020-1031.
doi: 10.2514/1.C031525

[4] Padfield, G. D., "The Making of Helicopter Flying Qualities; A Requirements Perspective," *The Aeronautical Journal*, Vol. 102, No. 1018, Dec. 1998, pp. 409-437.
doi: 10.1017/S0001924000027627

[5] Advani, S. K., and Wilkinson, C. H., "Dynamic Interface Modelling and Simulation: A Unique Challenge," *Royal Aeronautical Society Conference on Helicopter Flight Simulation*, London, Nov. 2001.

[6] Roscoe, M. F., and Wilkinson, C. H., "DIMSS-JSHIP's M&S Process for Ship Helicopter Testing and Training," *AIAA Modeling and Simulation Technologies Conference and Exhibit*, AIAA Paper 2002-4597, Aug. 2002.
doi: 10.2514/6.2002-4597

[7] Healey, J. V., "Simulating the Helicopter-Ship Interface as an Alternative to Current Methods of Determining the Safe Operating Envelopes," Naval Postgraduate School Report, NPS-67-86-003, Monterey, CA., Sep. 1986, pp. 48-58.

[8] Hoencamp, A., and Pavel, M. D., "Concept of a Predictive Tool for Ship–Helicopter Operational Limitations of Various In-Service Conditions," *Journal of the American Helicopter Society*, Vol. 57, No. 3, July 2012, pp. 1-9.
doi: 10.4050/JAHS.57.032008

[9] Fitzjohn, D., Turner, G. P., and Padfield, G. D., "The Use of Modelling and Simulation in Support of First of Class Flying Trials," *24th European Rotorcraft Forum*, Marseilles, France, Sep. 1998.

[10] Scott, P., Kelly, M. F., White, M. D. and Owen, I., "Using Piloted Simulation to Measure Pilot Workload of Landing a Helicopter on a Small Ship," *43rd European Rotorcraft Forum*, Vol.1, Milan, Italy, Sep. 12-15, 2017, pp. 704-713.

[11] Hodge, S. J., Forrest, J. S., Padfield, G. D., and Owen, I., "Simulating the Environment at the Helicopter-Ship Dynamic Interface: Research, Development and Application," *The Aeronautical Journal*, Vol. 116, No. 1185, Nov. 2012, pp. 1155-1184.
doi: 10.1017/S0001924000007545

[12] Padfield, G. D., and Wilkinson, C. H., "Handling Qualities Criteria for Maritime Helicopter Operations," *53rd American Helicopter Society Annual Forum*, Vol. 2, Virginia Beach, Virginia, April-May 1997, pp. 1425-1440.

[13] Kelly, M. F., White, M. D., Owen, I., and Hodge, S. J., "Piloted Flight Simulation for Helicopter Operation to the Queen Elizabeth Class Aircraft Carriers," *43rd European Rotorcraft Forum*, Vol. 1, Milan, Italy, Sep. 2017, pp. 659-669.

[14] Owen, I., White, M. D., Padfield, G. D., and Hodge, S., "A Virtual Engineering Approach to the Ship-Helicopter Dynamic Interface; A Decade of Modelling and Simulation Research at the University of Liverpool," *The Aeronautical Journal*, Vol. 49, No. 1246, Dec. 2017, pp. 1833-1857.

doi: 10.1017/aer.2017.102

[15] Kelly, M. F., Watson, N. A., Hodge, S. J., White, M. D., and Owen, I., “The Role of Modelling and Simulation in the Preparations for Flight Trials Aboard the Queen Elizabeth Class Aircraft Carriers,” *14th International Naval Engineering Conference*, Glasgow, UK, Oct. 2018.
doi: 10.24868/issn.2515-818X.2018.037

[16] White, M. D., Perfect, P., Padfield, G. D., Gubbels, A. W., and Berryman, A. C., “Acceptance Testing And Commissioning of a Flight Simulator for Rotorcraft Simulation Fidelity Research,” *Institution of Mechanical Engineers, Part G: Journal of Aerospace Engineering*, Vol. 227, No. 4, June 2012, pp. 663–686.
doi: 10.1177/0954410012439816

[17] Du Val, R., and He, C., “Validation of the FLIGHTLAB Virtual Engineering Toolset,” *The Aeronautical Journal*, Vol. 122, No. 1250, March 2018, pp. 519-555.
doi: 10.1017/aer.2018.12

[18] Beck, C. P., and Funk, J. D., “Development and Validation of a Seahawk Blade Element Helicopter Model in Support of Rotorcraft Shipboard Operations,” *RAeS Rotorcraft Group conference on Rotorcraft Simulation*, London, UK, May 1994.

[19] Memon, W. A., White, M. D., Owen, I., and Robinson, S., “Preliminary Progress in Establishing Motion Fidelity Requirements for Maritime Rotorcraft Flight Simulators,” *74th American Helicopter Society Annual Forum & Technology Display*, Vol. 1, Phoenix, Arizona, USA, May 2018, pp. 627-641.

[20] Memon, W. A., Owen, I., and White, M. D., “Motion Fidelity Requirements for Helicopter-Ship Operations in Maritime Rotorcraft Flight Simulators,” *Journal of Aircraft*. (Accepted for publication, under production).
doi: 10.2514/1.C035521

[21] Memon, W. A., White, M. D., and Owen, I., “Visual-Vestibular Motion Cueing Assessment in Maritime Rotorcraft Flight Simulators,” *45th European Rotorcraft Forum*, Warsaw, Poland, Sep. 2019.

[22] Anon., “Aeronautical Design Standard Performance Specification Handling Qualities Requirements for Military Rotorcraft,” ADS-33E-PRF, United States Army Aviation and Missile Command, Redstone Arsenal, AL, 2000.

[23] Lee, D., and Horn, J. F., “Simulation of Pilot Workload for a Helicopter Operating in a Turbulent Ship Airwake,” *Proceedings of the Institution of Mechanical Engineers, Part G: Journal of Aerospace Engineering*, Vol. 219, No. 5, May 2005, pp. 445–458.
doi: 10.1243/095441005X30298

[24] Moon, J., Domercant, J. C., and Mavris, D., “A Simplified Approach to Assessment of Mission Success for Helicopter Landing on a Ship,” *International Journal of Control, Automation and Systems*, Vol. 13, No. 3, Aug. 2014, pp. 680-688.
doi: 10.1007/s12555-013-0092-y

[25] Jarrett, D., and Manso, S., “Validation of Simulated Ship Air wake Effects on Helicopter Recoveries,”

73rd American Helicopter Society Annual Forum and Technology Displays, Vol. 4, Fort Worth, Texas, USA, May 2017, pp. 2786-2797.

[26] Figueira, J. M. P., Taghizad, A., and Abid, M., "The use of Simulation Tools to Estimate Ship-Helicopter Operating Limitations," *AIAA Modeling and Simulation Technologies Conference*, AIAA Paper 2017-4331, June 2017.
doi: 10.2514/6.2017-4331

[27] Xu, S., Tan, W., Efremov, A. V., Sun, L., and Qu, X., "Review of Control Models for Human Pilot Behaviour," *Annual Reviews in Control*, Vol. 44, Oct. 2017, pp. 274-291.
doi: 10.1016/j.arcontrol.2017.09.009

[28] Hess, R. H., "A Simplified Technique for Modelling Piloted Rotorcraft Operations Near Ships," *Journal of Guidance, Control, and Dynamics*, Vol. 29, No. 6, Nov.–Dec. 2006, pp. 1339–1349.
doi: 10.2514/1.18711

[29] Carignan, S., Gubbels, A., and Ellis, K., "Assessment of Handling Qualities for the Shipborne Recovery Task ADS 33 (Maritime)," *56th American Helicopter Society Annual Forum*, Vol. 2, Virginia Beach, VA, May 2000, pp. 814-824.

[30] Heenan, M. L., Scheidt, R. A., and Beardsley, S. A., "Visual and Proprioceptive Contributions to Compensatory and Pursuit Tracking Movements in Humans," *33rd Annual International Conference of the IEEE EMBS*, Vol. 1, Boston, Massachusetts USA, Aug.-Sept. 2011, pp. 7356-7359.
doi: 10.1109/IEMBS.2011.6091839

[31] John, W. S., and Marianne, C., "Tracking Performance on Combined Compensatory and Pursuit Tasks," WADC TR 52-39, 1952.

[32] Hess, R. A., "Simplified Approach for Modelling Pilot Pursuit Control Behaviour in Multi-Loop Flight Control Tasks," *Institution of Mechanical Engineers, Part G: Journal of Aerospace Engineering*, Vol. 220, No. 2, Feb. 2006, pp. 85–102.
doi: 10.1243/09544100JAERO33

[33] Hess, R. H., "Model for Human Use of Motion Cues in Vehicular Control". *Journal of Guidance, Control, and Dynamics,* Vol. 13, No. 3, 1990, pp. 476-482.
doi: 10.2514/3.25360

[34] Hosman, R. J. A. W., Cardullo, F. M., and Bos, J. E., "Visual-Vestibular Interaction in Motion Perception," *AIAA Modelling and Simulation Technologies Conference*, AIAA Paper 2011-6425, Oregon, Aug. 2011.
doi: 10.2514/6.2011-6425

[35] Hess, R. H., and Marchesi, F., "Analytical Assessment of Flight Simulator Fidelity Using Pilot Models," *Journal of Guidance, Control, and Dynamics,* Vol. 32, No. 3, May-June 2009, pp. 760-770.
doi: 10.2514/1.40645

[36] Nash, C. J., Cole, D. J., and Bigler, R. S., "A Review of Human Sensory Dynamics for Application to Models of Driver Steering," *Biological Cybernetics*, Vol. 110, Nos. 2-3, April 2016, pp. 91–116.

doi: 10.1007/s00422-016-0682-x

[37] Aman, J. E., Elangovan, N., Yeh, I. L., and Konczak, J., “The effectiveness of proprioceptive training for improving motor function: A systematic review,” *Frontiers in Human Neuroscience*, Vol. 8, No. 1075, Jan. 2015, pp. 1–18.
doi: 10.3389/fnhum.2014.01075

[38] Hess, R. A., and Siwakosit, W., “Assessment of Flight Simulator Fidelity in Multiaxis Tasks Including Visual Cue Quality,” *Journal of Aircraft*, Vol. 38, No. 4, July-Aug. 2001, pp. 607–614.
doi: 10.2514/2.2836

[39] Hess, R. A., “Obtaining Multi-Loop Pursuit-Control Pilot Models from Computer Simulation,” *Institution of Mechanical Engineers, Part G: Journal of Aerospace Engineering*, Vol. 222, No. 2, Feb. 2008, pp. 189–200.
doi: 10.1243/09544100JAERO260

[40] Lusardi, J. A., Tischler, M. B., Blanken, C. L., and Labows, J. S., “Empirically Derived Helicopter Response Model and Control System Requirements for Flight in Turbulence,” *Journal of the American Helicopter Society*, Vol. 49, No. 3, July 2004, pp. 340-349.
doi: 10.4050/JAHS.49.340

[41] Lusardi, J. A., "Control Equivalent Turbulence Inputs Model for the UH-60,” Ph.D. Dissertation, Department of Mechanical and Aeronautical Engineering, University of California, Davis, CA, 2004.

[42] McTaggart, K., “Validation of ShipMo3D Version 1.0 User Applications for Simulation of Ship Motion,” Technical Memorandum, DRDC Atlantic TM 2007-173, Aug. 2007.

[43] Tischler, M. B., and Cauffman, M. G., “Comprehensive Identification from Frequency Responses: Volume 1 - Class Notes,” NASA CP 10149, USAATCOM TR-94-A-017, 1994.

[44] Klee, H., and Allen, R., “Simulation of Dynamic Systems with MATLAB and Simulink,” CRC Press, Orlando, USA, 2016, pp. 561.

Appendix: Flight Dynamics Models

1. Hover Dynamics

$$A = \begin{bmatrix} -0.0005 & 0.0179 & 0 & 0 & 0 & 0 & 1 & -0.0023 & 0.043 \\ -0.018 & 0 & 0 & 0 & 0 & 0 & 0 & 0.99 & 0.0532 \\ -0.0104 & 0.0008 & 0 & 0 & 0 & 0 & 0 & -0.0533 & 0.99 \\ 0 & -28.625 & 0 & -0.0178 & 0.0066 & 0.02235 & -1.677 & 3 & 0.0551 \\ 32.1243 & -0.3183 & 0 & -0.0041 & -0.0278 & 0 & -1.754 & -1.82 & 0.896 \\ 1.7133 & -1.1962 & 0 & 0.0031 & -0.0325 & -0.252 & -0.6834 & 0.25 & 1.44 \\ 0.0001 & -0.4518 & 0 & 0.0261 & -0.0231 & -0.0002 & -4.53 & -1.73 & -0.0138 \\ -0.0001 & -0.6826 & 0 & 0.003 & 0.0056 & 0.0022 & 0.223 & -0.98 & -0.044 \\ -0.0001 & -0.0227 & 0 & 0.0013 & 0.0033 & 0.0001 & -0.185 & -0.146 & -0.186 \end{bmatrix}$$

$$B = \begin{bmatrix} 0 & 0 & 0 & 0 \\ 0 & 0 & 0 & 0 \\ 0 & 0 & 0 & 0 \\ 0 & -0.165 & 0 & 0 \\ 0.0915 & 0 & 0 & 0 \\ 0.0003 & -0.0093 & -0.0548 & 0 \\ 0.1152 & 0 & 0 & 0 \\ 0 & 0.0318 & 0 & 0 \\ 0 & 0 & 0 & 0.0196 \end{bmatrix}$$

2. Forward Flight Dynamics

$$A = \begin{bmatrix} 0 & 0 & 0 & 0 & 0 & 0 & 1 & -0.0014 & 0.0522 \\ 0 & 0 & 0 & 0 & 0 & 0 & 0 & 0.999 & 0.0274 \\ 0 & 0 & 0 & 0 & 0 & 0 & 0 & -0.0274 & 1.001 \\ -0.0058 & -28.2488 & 0.1384 & -0.0163 & 0.0443 & 0.0245 & -1.7949 & 2.7805 & -0.4359 \\ 32.0624 & -0.0997 & 1.4544 & 0.0282 & -0.0629 & 0.0099 & -1.2172 & -1.7431 & -19.32 \\ 0.8395 & -9.1248 & 2.1489 & -0.1188 & -0.8202 & -0.4906 & 6.7447 & 22.24 & 4.268 \\ -0.0273 & 0.1559 & 0.5531 & 0.0318 & -0.0448 & 0.0264 & -4.9511 & -1.6605 & 0.0929 \\ 0.0055 & -0.716 & -0.1416 & 0.0016 & 0.0058 & -0.0007 & 0.0925 & -1.3144 & -0.0667 \\ 0.0124 & -0.0237 & -0.2156 & -0.0065 & 0.0127 & -0.0015 & -0.3826 & -0.0732 & -0.4269 \end{bmatrix}$$

$$B = \begin{bmatrix} 0 & 0 & 0 & 0 \\ 0 & 0 & 0 & 0 \\ 0 & 0 & 0 & 0 \\ 0.0062 & -0.1561 & -0.0067 & 0.0558 \\ 0.0914 & 0.013 & -0.0106 & -0.0645 \\ -0.0363 & -0.0894 & 0.2155 & -0.0413 \\ 0.114 & 0.0167 & 0.0093 & -0.0304 \\ 0.0001 & 0.0304 & 0.0003 & -0.0015 \\ 0.005 & 0.0003 & -0.0021 & 0.022 \end{bmatrix}$$